

Draftable Comparison Export

This document is an exported comparison with limited functionality, generated by Draftable Desktop. To access full functionality, use Draftable's powerful comparison viewer in any of our products.

Left document: metroatomotive_VIAQ__Special_Issue_on_MDPI_Sensors__major_revisions.pdf

Right document: Air_Quality_and_Comfort_Characterisation_within_an_Electric_Vehicle_Cabin_in_Heating_and_Cooling_Operations__2nd_round.pdf

What is this document?

This is a comparison of two documents. The two documents are interleaved such that the left document is displayed on even pages and the right document is displayed on odd pages.

Is there a specific way I should view this file?

This document is intended to be viewed in Two Page Continuous mode (or sometimes called 'Two Page Scrolling'). It should open in this mode by default when using Adobe Acrobat and most popular PDF readers.

If the document opens in a different view, you can often change this in the settings. In Adobe Acrobat, go to **View > Page Display > Two Page Scrolling**.

Why are there blank pages?

Blank pages are inserted to keep both documents as aligned as much as possible.

How do I read the changes?

Text deleted from the left document and, hence, not in right document is highlighted red. Text added to the right document and, hence, not in left document is highlighted green.

Tip for printing

When printing this document, we recommend printing double-sided and include this first page. This will result in the matching text being displayed on different pages and easily readable, much like a book.

For more information

Draftable offers powerful document comparison solutions for all use-cases. To view our products, please visit our website: draftable.com.

Characterisation of Comfort and Air Quality in an Electric Vehicle in Heating and Cooling Operations[†]

Luigi Russi ^{1,‡,*}, Paolo Guidorzi ¹, Beatrice Pulvirenti ¹,
Davide Aguiari ², Giovanni Pau²¹ and Giovanni Semprini ¹

¹ Department of Industrial Engineering, Alma Mater Studiorum, University of Bologna; luigi.russi@unibo.it

² Department of Computer Science and Engineering, Alma Mater Studiorum, University of Bologna; davide.aguiari2@unibo.it

* Correspondence: luigi.russi@unibo.it

† This paper is an extended version of [1]

‡ Current address: Viale del Risorgimento 2, 40136, Bologna, Italy

Abstract: This work is aimed at the experimental characterisation of air quality within a vehicle cabin, by measuring at the same time the HVAC system energy consumption. Pollutant concentrations in the vehicle cabin are measured by means of a low-cost system of sensors. The effects of the HVAC system configuration on the cabin air quality are discussed, such as fresh-air and recirculation mode. It is shown that the PM concentrations obtained in the recirculation mode are lower than those obtained in fresh-air mode, while the VOC concentrations obtained in the recirculation mode are higher than those obtained in fresh-air mode. The energy consumption is measured in relation to the configuration of the HVAC system and the measured concentrations. The novelty of this work is the combined measurement of important comfort parameters such as temperature distribution and air quality within the vehicle and the real time energy consumption of the HVAC system. A wider concept of comfort is enabled, based on the use of low-cost sensors in the automotive field.

Keywords: Electric vehicle, pollutant concentration, HVAC, Arduino sensors, vehicle energetics

1. Introduction

This paper describes a series of experimental readings of air quality and energy efficiency inside the passenger compartment of a car. The measurements were carried out using low cost sensor systems and connecting to the car's On-Board Diagnostic bus (OBD) [1]. The temperature and the other environmental parameters inside the vehicle's enclosure are affected by outside weather conditions as well as by the Heating, Ventilation, and Air Conditioning (HVAC) working state. Reducing the power consumption of the HVAC system, as well as other secondary systems of course, is of paramount importance in this era of migration to electric powered transportation, and the major challenge is to achieve this while maintaining high levels of comfort in the cabin. The best thermal management in the cabin of the car is obtained by maximizing comfort level along with minimizing electrical power demand. For example, choosing the intake air recirculation mode is recommended under certain conditions to economize energy and increase driving duration. EPA released fuel credits with the growth of re-circulation of air in 2017. The energy benefits of the recirculation mode are undisputed, but there are some points to consider: CO₂ and VOC accumulation, pollutant infiltration and odour problems. Cabin air quality, especially when air is re-circulating, should be measured and regulated to keep concentrations of certain pollutants below specific thresholds [2]. It should also be mentioned that air re-circulation can produce substantial benefits in relation to certain air contaminants, which are captured by HVAC filters. Research in the field of vehicle air quality is leading to new methods of testing and best practices, but

Citation: Title. *Sensors* **2021**, *1*, 0.
<https://doi.org/>

Received:

Accepted:

Published:

Publisher's Note: MDPI stays neutral with regard to jurisdictional claims in published maps and institutional affiliations.

Copyright: © 2021 by the authors. Submitted to *Sensors* for possible open access publication under the terms and conditions of the Creative Commons Attribution (CC BY) license (<https://creativecommons.org/licenses/by/4.0/>).

Air Quality and Comfort Characterisation within an Electric Vehicle Cabin in Heating and Cooling Operations[†]

Luigi Russi ^{1,‡,*}, Paolo Guidorzi ¹, Beatrice Pulvirenti ¹,
Davide Aguiari ², Giovanni Pau²¹ and Giovanni Semprini ¹

¹ Department of Industrial Engineering, Alma Mater Studiorum, University of Bologna; luigi.russi@unibo.it

² Department of Computer Science and Engineering, Alma Mater Studiorum, University of Bologna; davide.aguiari2@unibo.it

* Correspondence: luigi.russi@unibo.it

† This paper is an extended version of [1]

‡ Current address: Viale del Risorgimento 2, 40136, Bologna, Italy

Abstract: This work is aimed at the experimental characterisation of air quality and thermal profile within an electric vehicle cabin, measuring at the same time the HVAC system energy consumption. Pollutant concentrations in the vehicle cabin are measured by means of a low-cost system of sensors. The effects of the HVAC system configuration, such as fresh-air and recirculation mode, on cabin air quality are discussed. It is shown that the PM concentrations observed in recirculation mode are lower than those in fresh-air mode, while VOC concentrations are generally higher in recirculation than in fresh-air mode. The energy consumption is compared in different configurations of the HVAC system. The novelty of this work is the combined measurement of important comfort parameters such as air temperature distribution and air quality within the vehicle, together with the real time energy consumption of the HVAC system. A wider concept of comfort is enabled, based on the use of low-cost sensors in the automotive field.

Keywords: Electric vehicle, pollutant concentration, HVAC, Arduino sensors, vehicle energetics

1. Introduction

One of the major barriers to electric vehicle adoption is due to the limited amount of energy stored in the batteries and needed for traction and auxiliary systems. While ICE vehicles can rely on waste heat for winter requirements, an optimised thermal management of heat loads and gains is crucial for BEVs, paving the way from heat disposal to heat management [2].

Reducing the energy consumption of the HVAC system, as well as other auxiliary systems is of paramount importance in the era of migration to electric powered transportation; the major challenge being to achieve this while maintaining high levels of comfort inside the cabin. On one hand, the best thermal management of the car's cabin is obtained by maximising comfort level along with minimising electrical power demand [3–5]. On the other hand, internal air quality (IAQ) related quantities inside the vehicle's enclosure are affected by outside weather conditions as well as by the Heating, Ventilation, and Air Conditioning (HVAC) settings. From this perspective, every improvement of the cabin thermal management must be IAQ aware [6–9].

As an example, choosing the intake air recirculation mode is recommended under certain conditions to reduce energy use and increase driving range. Provided that energy benefits of the recirculation mode are undisputed, it should also be mentioned that it can produce substantial benefits in relation to certain air contaminants, which are captured by HVAC filters [10], but there are some downsides to consider: CO₂ and VOC accumulation, pollutant infiltration and odour problems. United States Environmental Protection Agency (EPA) released fuel credits to manufacturers adopting increased air

Citation: Title. *Sensors* **2021**, *1*, 0.
<https://doi.org/>

Received:

Accepted:

Published:

Publisher's Note: MDPI stays neutral with regard to jurisdictional claims in published maps and institutional affiliations.

Copyright: © 2021 by the authors. Submitted to *Sensors* for possible open access publication under the terms and conditions of the Creative Commons Attribution (CC BY) license (<https://creativecommons.org/licenses/by/4.0/>).

35 still a standard on performance indicators does not exist. Several efforts have been made
36 in order to define a standardized test method for automotive interior air quality [3], but
37 this is still an open question. The Joint Research Center of the European Commission
38 and DG Service Environment are pushing for advancement in this field by stimulating
39 research improvements achieved through the use of low-cost sensors. Although the
40 data measured with these types of sensors are less accurate than laboratory reference
41 equipment, their use has grown greatly in recent years, in applications concerning indoor
42 air quality (IAQ) [4]. This is due also to their ease of use, which makes them suitable
43 for real-time monitoring applications. The road has therefore been opened for the use
44 of low-cost sensors in the automotive sector, for monitoring the air quality inside the
45 passenger compartment. In this paper, the correlation between experimentally measured
46 air quality data and the energy spent by the HVAC system inside the vehicle cabin is
47 investigated. Concentrations of some pollutants in the vehicle cabin [5] are measured by
48 means of a low-cost Arduino sensor-based system [6]. The HVAC system configuration
49 and fresh air recirculation mode of the intake air are varied while PM2.5 and VOC
50 percentages are measured. HVAC air filter performance is evaluated by making cabin
51 air quality measurements with and without the filter installed. The relation between
52 consumed energy, HVAC system working state and pollutant concentrations is obtained
53 in order to investigate a new approach to comfort maintenance inside the car cabin, and
54 for optimizing the development of BEVs vehicles methodologies.

55 2. Materials and Methods

56 In the following subsections, the integrated experimental setup and the low-cost
57 sensors chosen are described.

58 2.1. Description of the experimental setup

59 To characterise the thermal profile and air quality inside the vehicle cabin, two tests
60 have been performed in real outdoor parking conditions. The vehicle was a 2018 Nissan
61 Leaf Acenta 40 kWh, parked in the faculty parking lot with the front of the car oriented
62 south.

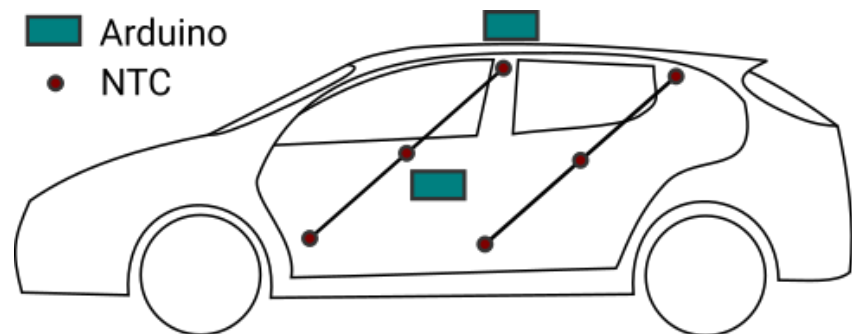


Figure 1. Lateral view of the experimental setup

63 The temperature distribution within the vehicle cabin is obtained with a grid of 18
64 DS18B20 temperature sensors following the approach used in [7] and [8] to develop a
65 thermal model of a BEV cabin for energy consumption predictions [9]. The cabin has
66 been ideally divided into three slices horizontally, namely top, middle and bottom level,
67 as shown in Fig. 1 from a lateral view.

68 On the grid, six sensors are placed on each plane: three in the front side and three in
69 the back side of the cabin. In addition, air quality related quantities have been measured
70 with low-cost sensors on a single location in the cabin; near the gear shift knob together
71 with the acquisition system.

72 As external conditions can strongly affect the internal micro-climate [10], a second
73 acquisition system has been placed on the car roof. This is identical to the internal one,
74 except for the presence of a single temperature sensor only. The presence of the second

35 recirculation in 2017; but cabin air quality, especially when air is recirculating, should
36 be measured and regulated to keep concentrations of certain pollutants below specific
37 thresholds [11,12].

38 Research in the field of vehicle air quality is leading to new methods of testing and
39 best practices, but still a dedicated standard on performance indicators does not exist.
40 Several efforts have been made to define a standardised test method for interior air qual-
41 ity in the automotive field [13], but this is still an open question. A possible approach to
42 address this issue relies on fractional air recirculation, demonstrating that a compromise
43 is achievable between the benefits of full recirculation and its side effects [14]. Other
44 authors propose approaches based on the use of a signal from environmental prediction
45 services [15], and/or on-board sensors [16] to trigger automatic climate control, even
46 though there is still no clear consensus on how to implement these techniques in the
47 HVAC system's control strategy. Such approach would require a trade-off between real
48 time and integral I/O techniques, the former leading to large uncertainties but faster,
49 while the latter provide slower but more stable results [17].

50 The Joint Research Centre of the European Commission and DG Service Environ-
51 ment are pushing for advancement in this field by stimulating research improvements
52 achieved through the use of low-cost sensors. Although the data measured with these
53 type of sensors are less accurate than laboratory reference equipment, their use has
54 grown greatly in recent years, in applications concerning indoor air quality [18]. Their
55 ease of use, coupled with current scientific advancements [19–21], makes them suitable
56 for real-time monitoring applications. The road has therefore been opened for the em-
57 ployment of low-cost sensors in the automotive sector, such as monitoring air quality
58 inside the passenger compartment.

59 This paper describes a series of experiments on air quality and energy efficiency
60 inside the passenger compartment of an electric vehicle. The measurements were carried
61 out using a portable low-cost sensor system and reading the car's On-Board Diagnostic
62 bus (OBD) [1]. In this work, the correlation between experimentally measured air quality
63 data and the energy spent by the HVAC system inside the vehicle cabin is investigated.
64 Concentrations of some pollutants in the vehicle cabin are measured by means of a
65 low-cost Arduino sensor-based system. The use of an open-source electronic platform
66 like Arduino allowed fast prototyping and simplified design of the system. In addition,
67 it helped to relax the constraint involved in the construction of hardware and software
68 platforms for data acquisition, following a path that has been outlined by many authors
69 in literature [22–24].

70 The HVAC system configuration regarding fresh-air recirculation mode of the
71 intake air are varied while PM_{2.5} and VOC percentages are measured. HVAC air filter
72 performance is evaluated by making cabin air quality measurements with and without
73 the filter installed. The relation between consumed energy, HVAC system settings and
74 pollutant concentrations is obtained, in order to introduce an innovative approach to
75 comfort maintenance inside the car cabin. The novelty of this approach is a win-win
76 perspective, aimed to the concurrent optimisation of the two aspects for BEVs thermal
77 control. The methodology, based on low-cost sensors measurements and applied to a
78 Nissan Leaf Acenta 40 kWh MY2018, is general and applicable to other models of electric
79 car, to show that the use of these sensors for the control of the cabin can yield energy
80 saving together with an optimal air quality and comfort levels.

81 2. Materials and Methods

82 In the following subsections, the integrated experimental setup and the low-cost
83 system of sensors are described in detail.

75 acquisition system is needed to characterize the environment outside the vehicle and
 76 to facilitate inside/outside comparisons with data having the same structure and same
 77 metrologic fingerprint.

78 The approach used in the study, conversely from the one used in ISO standards
 79 regarding interior air of road vehicles [11], does not rely on a vehicle test chamber. The
 80 latter being well documented and reliable, but not suitable for real-time operation and
 81 low-cost equipment.

82 To have clearer insights on HVAC capabilities, an On-Board Diagnostic (OBD) Linux
 83 platform was cleverly installed inside the car to directly retrieve and collect different
 84 variables from the electronic control units [12]. Specifically, it was the *iWave OBD-II*: a
 85 little device with an *ARM Cortex-A7* processor embedded that runs a light *Yocto Poky*
 86 Linux distribution. The *iWave OBD-II* can upload data via a 4G/LTE CAT4/CAT1 sim
 87 modem, geolocate the device with a GPS receiver and it can transmit messages with the
 88 Bluetooth Low Energy 4.2 module. Communicating via the OBD-II interface, the board
 89 reads the HVAC power consumption, the power used by the auxiliary equipment (e.g.
 90 lights, infotainment, rear defroster etc.), and the power used by the heater. A fine-time
 91 granularity monitoring of those parameters was necessary to correctly interpret how the
 92 cabin air changes throughout the experiment.

93 The overall measured quantities are: air temperature t_a , relative humidity RH , air
 94 pressure p_a , TVOC concentration C_{TVOC} and $PM_{2.5}$ concentration C_{PM} . The temperature
 95 is measured in 18 points as described above, while the other measurements are taken in
 96 one point. The same quantities are measured also outside the cabin. Finally, the power
 97 usage of the HVAC system is also logged. Table 1 lists the measured quantities and the
 98 correspondent accuracy.

Table 1. Measured quantities.

Variable (Unit)	Description	Specifications	
		Sensor	Accuracy (offset + gain)
t_a (°C)	Air temp.	DS18B20	$\pm(0.5\text{ }^\circ\text{C} + 1\%mv^a)$
RH (%)	Air rel. hum.	BME280	$\pm(3\%RH + 1\%RH)$
p_a (hPa)	Air pres.	BME280	$\pm(1.5\text{ hPa} + 0.12\text{ hPa})$
TVOC (ppb)	TVOC conc.	SGP30	$\pm(15\%mv)$
$PM_{2.5}$ ($\mu\text{g}/\text{m}^3$)	$PM_{2.5}$ conc.	SPS30	$\pm(10\ \mu\text{g}/\text{m}^3 + 10\%mv)$
P_i (kW)	Subsystem i power usage	OBD/Linux	$\pm(250\text{ W})$

^a mv = measured value.

99 Sensor performance is a device dependent issue that can be measured with various
 100 qualifiers [13] and ideally addressed individually. In this study, the same approach for
 101 all the measured quantities has been used. A sampling time of $T_s = 10$ seconds has been
 102 adopted. The raw data from the acquisition system have been filtered with a moving
 103 mean over a 1 minute period, this leads to a 6 point moving mean. Subsequently, the
 104 filtered data have been converted to time-stamped data in tabular form, and eventually
 105 re-sampled and synchronized among the three acquisition systems. The data analysis
 106 process has been performed using open source tools, python 3.8 and several scientific
 107 computing libraries (pandas, matplotlib, numpy and scipy above all) following the
 108 exploratory data analysis (EDA) approach provided in [14].

109 2.2. Description of the Arduino-based system of sensors

110 Two independent measurement systems based on Arduino Mega 2560 were built
 111 for the measurement of environmental parameters. The systems have an on-board Real
 112 Time Clock (RTC), a data logger on flash memory, a fan and a TFT display. The RTC
 113 clocks of the two systems are constantly adjusted thanks to time data received from the

2.1. Description of the experimental setup

To characterise the thermal profile and air quality inside the vehicle cabin, two tests have been performed in outdoor parking conditions in the faculty parking lot with the front of the car oriented south.

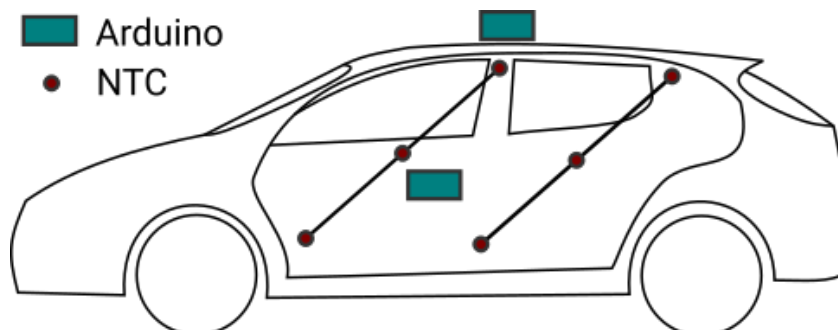


Figure 1. Lateral view of the experimental setup

The temperature distribution within the vehicle cabin is obtained with a grid of 18 DS18B20 temperature sensors following the approach used in [25] and [26] to develop a thermal model of a BEV cabin for energy consumption predictions [27]. The cabin has been ideally divided into three slices horizontally, namely top, middle and bottom level, as shown in Fig. 1 from a lateral view.

On the grid, six sensors are placed for each plane: three in the front side and three in the back side of the cabin. In addition, air quality related quantities have been measured with low-cost sensors on a unique location in the cabin; near the gear shift knob together with the acquisition system.

As external conditions can strongly affect the internal micro-climate [28], a second acquisition system has been placed on the car roof. This is identical to the internal one, except for the presence of a single temperature sensor only. The presence of the second acquisition system is needed to characterise the environment outside the vehicle and to facilitate inside/outside comparisons with data having the same structure and same metrologic fingerprint.

The approach used in the study, conversely from the one used in ISO standards regarding interior air of road vehicles [29], does not rely on a vehicle test chamber. The latter being well documented and reliable, but not suitable for real-time operation and low-cost equipment.

To have clearer insights on HVAC capabilities, an On-Board Diagnostic (OBD) Linux platform was cleverly installed inside the car to directly retrieve and collect different variables from the electronic control units [30]. Specifically, it was the *iWave OBD-II*: a little device with an *ARM Cortex-A7* processor embedded that runs a light *Yocto Poky* Linux distribution. The *iWave OBD-II* can upload data via a 4G/LTE CAT4/CAT1 sim modem, geolocate the device with a GPS receiver and it can transmit messages with the Bluetooth Low Energy 4.2 module. Communicating via the OBD-II interface, the board reads the HVAC power consumption, the power used by the auxiliary equipment (e.g., lights, infotainment, rear defroster etc.), and the power used by the heater. A fine-time granularity monitoring of those parameters was necessary to correctly interpret how the cabin air changes throughout the experiment.

The overall measured quantities are: air temperature t_a , relative humidity RH , air pressure p_a , TVOC concentration C_{TVOC} and $PM_{2.5}$ concentration C_{PM} . The temperature is measured in 18 points as described above, while the other measurements are taken in one point. The same quantities are measured also outside the cabin. Finally, the power usage of the HVAC system is also logged. Table 1 lists the measured quantities and the correspondent accuracy.

Sensor performance is a device dependent issue that can be measured with various qualifiers [31] and ideally addressed individually. In this study, the same approach for

114 GPS module. This operation is implemented to facilitate the synchronization of signals
115 from the three acquisition systems.

116 The internal system is capable of measuring temperatures at 18 locations in the
117 cabin (Maxim Integrated DS18B20 probes). Moreover, the internal system can measure
118 Particulate air Matter (PM) concentration (Sensirion SPS30 sensor), air TVOC concentra-
119 tion (Sensirion SGP30 sensor), air CO₂ concentration (Winsen MH-Z19B non-dispersive
120 infrared sensor), concentration formaldehyde (Winsen ZE08 sensor), air temperature,
121 relative humidity and pressure (Bosch BME280 sensor), air flow velocity (hot wire analog
122 sensor) and GPS position, at a **single** location. The external system, albeit sharing the
123 same characteristics and using the same sensors, it lacks of the 18-spots temperature mea-
124 surement, the GPS receiver and the air flow velocity sensor. Both systems are equipped
125 with a fan that conveys air inside the device enclosure, where CO₂ and formaldehyde
126 sensors are mounted, while the SPS30 sensor is equipped with its built-in fan. Both
127 systems independently sampled data at 10-second intervals. All digital sensors used in
128 the measurement device include a microcontroller that implements optimization and
129 self-calibration algorithms.

130 High-precision, easy-to-use DS18B20 sensors were used to measure temperatures
131 inside the cabin in 18 **different** positions; they have a typical accuracy of $\pm 0.5^\circ\text{C}$ from
132 -10°C to $+85^\circ\text{C}$ and digitally transmit temperature data on a 1-Wire[®] bus. The use of
133 1-Wire protocol [15], together with the unique 64-bit serial code allows many sensors **on**
134 the same bus, thus reducing the cable length and allowing to uniquely associate a sensor
135 output with its position in the network trough a serial-position coupling. Specifically, the
136 DS18B20 actual temperature is provided by a 12-bit analog to digital converter built-in
137 in the digital sensor, with a fine temperature resolution up to 0.0625°C . Its operating
138 range is between -55°C to $+125^\circ\text{C}$.

139 The BME280 is a high linearity and high accuracy combined temperature, humid-
140 ity and pressure digital sensor. Its pressure sensing mechanism is resistive, with an
141 operation range of 300 hPa to 1100 hPa, temperature sensing principle is of the type
142 diode-voltage with a measurement range of -45°C to 85°C , measurement principle
143 behind humidity is capacitive and its range is 0 % to 100 % [16]. It features an extremely
144 fast response time $\tau_{63\%}$ of 1 s, thus enabling a consistent oversampling if compared with
145 the current application time granularity of min.

146 The sensing principle of SPS30 PM sensor is based on laser-scattering, and allows
147 mass concentration and number concentration sensing for particle sizes ranging from
148 $1\ \mu\text{m}$ to $10\ \mu\text{m}$. As discussed in [17] and [18], the SPS30 is an optical particle counter
149 (OPC) optimised for PM_{2.5} and smaller particle analysis. Sensirion PM sensors are in-
150 deed calibrated using regularly maintained and aligned high-end reference instruments
151 (e.g., the TSI Optical Particle Sizer Model 3330 or the TSI DustTrak[™] DRX 8533) only **for**
152 $2.5\ \mu\text{m}$ particles size. Moreover, as stated in the sensor specification **statement from the**
153 **producer**, PM₄ and PM₁₀ outputs are not directly measured but estimated from **smaller**
154 particle counts using typical aerosol profiles. A miniaturized fan and a High Efficiency
155 Particulate Air (HEPA) filter are included to reduce the optical part contamination; it also
156 runs its fan at full speed for 10 seconds every 7 days as an automatic cleaning procedure.
157 **Mass concentration measurement range: $0\ \mu\text{g}/\text{m}^3$ to $1000\ \mu\text{g}/\text{m}^3$.**

158 SGP30 TVOC sensor is a digital "multi-pixel" gas sensor. It uses multiple sensors,
159 housed on a single metal-oxide gas sensor chip, placed on a thermally controlled hotplate.
160 Digital data output from the sensor includes raw measurements of ethanol and H₂, and
161 calculated values of TVOC and equivalent CO₂ via internal algorithm, such as automatic
162 baseline compensation of the measurement [19]. The TVOC data range from this sensor
163 is between 0 to 60000 ppb. This sensor's equivalent CO₂ were disregarded due to its
164 low sensitivity to external pollutants and due to the absence of passengers in parking
165 conditions.

Table 1. Measured quantities.

Variable (Unit)	Description	Sensors specifications		
		Manufacturer	Model	Accuracy (offset + gain)
t_a (°C)	Air temp.	Maxim Integrated	DS18B20	$\pm(0.5\text{ }^\circ\text{C} + 1\%mv^a)$
RH(%)	Air rel. hum.	Bosch	BME280	$\pm(3\%RH + 1\%RH)$
p_a (hPa)	Air pres.	Bosch	BME280	$\pm(1.5\text{ hPa} + 0.12\text{ hPa})$
TVOC(ppb)	TVOC conc.	Sensirion	SGP30	$\pm(15\%mv)$
$PM_{2.5}$ ($\mu\text{g}/\text{m}^3$)	PM2.5 conc.	Sensirion	SPS30	$\pm(10\text{ }\mu\text{g}/\text{m}^3 + 10\%mv)$
P_i (kW)	Subsystem i power usage	iWave	OBD/Linux	$\pm(250\text{ W})$

^a mv = measured value.

all the measured quantities has been used. A sampling time of $T_s = 10$ seconds has been adopted. The raw data from the acquisition system has been filtered with a moving mean over a 1-minute period, this leads to a 6-point moving mean. Subsequently, the filtered data has been converted into time-stamped data in tabular form, and eventually re-sampled and synchronised among the three acquisition systems. The data analysis process has been performed using open-source tools, python 3.8 and several scientific computing libraries (pandas, matplotlib, numpy and scipy above all) following the exploratory data analysis (EDA) approach provided in [32].

2.2. Description of the Arduino-based system of sensors

Two independent measurement systems based on Arduino Mega 2560 were built for the measurement of environmental parameters. The systems have an on-board Real Time Clock (RTC), a data logger on flash memory, a fan and a TFT display. The RTC clocks of the two systems are constantly adjusted thanks to time data received from the GPS module. This operation is implemented to facilitate the synchronization of signals from the three acquisition systems.

The internal system is capable of measuring temperatures at 18 locations in the cabin (Maxim Integrated DS18B20 probes). Moreover, the internal system can measure Particulate air Matter (PM) concentration (Sensirion SPS30 sensor), air TVOC concentration (Sensirion SGP30 sensor), air CO₂ concentration (Winsen MH-Z19B non-dispersive infrared sensor), concentration formaldehyde (Winsen ZE08 sensor), air temperature, relative humidity and pressure (Bosch BME280 sensor), air flow velocity (hot wire analog sensor) and GPS position, at a unique location. The external system, albeit sharing the same characteristics and using the same sensors, it lacks of the 18-spots temperature measurement, the GPS receiver and the air flow velocity sensor. Both systems are equipped with a fan that conveys air inside the device enclosure, where CO₂ and formaldehyde sensors are mounted, while the SPS30 sensor is equipped with its built-in fan. Both systems independently sampled data at 10-second intervals. All digital sensors used in the measurement device include a microcontroller that implements optimisation and self-calibration algorithms.

High-precision, easy-to-use DS18B20 sensors were used to measure temperatures inside the cabin in 18 distinct positions; they have a typical accuracy of $\pm 0.5\text{ }^\circ\text{C}$ from $-10\text{ }^\circ\text{C}$ to $85\text{ }^\circ\text{C}$ and digitally transmit temperature data on a 1-Wire[®] bus. The use of 1-Wire protocol [33], together with the unique 64-bit serial code allows many sensors on the same bus, thus reducing the cable length and allowing to uniquely associate a sensor output with its position in the network through a serial-position coupling. Specifically, the DS18B20 actual temperature is provided by a 12-bit analog to digital converter built-in in the digital sensor, with a fine temperature resolution up to $0.0625\text{ }^\circ\text{C}$. Its operating range is between $-55\text{ }^\circ\text{C}$ to $125\text{ }^\circ\text{C}$.

The BME280 is a high linearity and high accuracy combined temperature, humidity and pressure digital sensor. Its pressure sensing mechanism is resistive, with an

166 operation range of 300 hPa to 1100 hPa, temperature sensing principle is of the type
167 diode-voltage with a measurement range of $-45\text{ }^{\circ}\text{C}$ to $85\text{ }^{\circ}\text{C}$, measurement principle
168 behind humidity is capacitive and its range is 0 % to 100 % [34]. It features an extremely
169 fast response time $\tau_{63\%}$ of 1 s, thus enabling a consistent oversampling if compared with
170 the current application time granularity of 1 min.

171 The sensing principle of SPS30 PM sensor is based on laser-scattering, and allows
172 mass concentration and number concentration sensing for particle sizes ranging from
173 $1\text{ }\mu\text{m}$ to $10\text{ }\mu\text{m}$. As discussed in [35] and [21], the SPS30 is an optical particle counter
174 (OPC) optimised for PM2.5 and smaller particle analysis. Sensirion PM sensors are in-
175 deed calibrated using regularly maintained and aligned high-end reference instruments
176 (e.g., the TSI Optical Particle Sizer Model 3330 or the TSI DustTrak™ DRX 8533) only
177 for $2.5\text{ }\mu\text{m}$ particles size. Moreover, as stated in the sensor specification sheet from the
178 manufacturer, PM4 and PM10 outputs are not directly measured but estimated from
179 smaller particle counts using typical aerosol profiles. A miniaturized fan and a High
180 Efficiency Particulate Air (HEPA) filter are included to reduce the optical part contam-
181 ination; it also runs its fan at full speed for 10 seconds every 7 days as an automatic
182 cleaning procedure. Mass concentration measurement range: $0\text{ }\mu\text{g}/\text{m}^3$ to $1000\text{ }\mu\text{g}/\text{m}^3$.

183 SGP30 TVOC sensor is a digital "multi-pixel" gas sensor. It uses multiple sensors,
184 housed on a single metal-oxide gas sensor chip, placed on a thermally controlled hotplate.
185 Digital data output from the sensor includes raw measurements of ethanol and H_2 , and
186 calculated values of TVOC and equivalent CO_2 via internal algorithm, such as automatic
187 baseline compensation of the measurement [19]. The TVOC data range from this sensor
188 is between 0 to 60000 ppb. This sensor's equivalent CO_2 were disregarded due to its
189 low sensitivity to external pollutants and due to the absence of passengers in parking
190 conditions.

191 The measurement system has been characterised both in winter and in summer
192 conditions. In the following sections, two typical conditions for winter and summer
193 have been chosen, to characterise the HVAC system performance in heating and cooling
194 operations, respectively. Winter tests have been performed on January 29, 2021, while
195 summer test have been carried out from July 14 to July 15, 2021.

196 3. Results and discussion

197 In this section, the combined measures of air quality and comfort parameters,
198 together with the energy consumption by the electric car are shown and discussed in
199 different seasons, in order to show the differences in relation to the operational mode
200 for the air conditioning. Moreover, an estimation of the filtration performances of the
201 HVAC system is given, by comparing the results corresponding to new and used filters.

202 3.1. Measurements during heating operation

203 Two different test conditions have been investigated, for the winter, starting from a
204 state of equilibrium with the external environment, obtained maintaining all systems off
205 and all doors opened for 15 minutes. Once the equilibrium was reached, the proper test
206 was performed while maintaining the heater on for 1 hour, the set-point temperature
207 at its maximum of $30\text{ }^{\circ}\text{C}$, the fan speed at its maximum (position 7), all the windows
208 and all the doors closed. During the first test, the recirculation system was off (meaning
209 that the air ventilation system was in fresh-air configuration), during the second test the
210 recirculation system was instead on.

211 3.1.1. Fresh-air configuration

212 The temperature measured inside and outside the cabin keeping the fresh-air mode
213 is shown in Fig. 2(a). The air temperature inside the cabin is obtained by the average
214 of the air temperature measurements on the sensors placed on the grid shown in Fig.
215 1, i.e., $t_{int} = t_{avg}$. The TVOC concentration measured inside and outside the cabin in
216 fresh-air mode are shown in Fig. 2(b). It is shown that the TVOC concentration increases

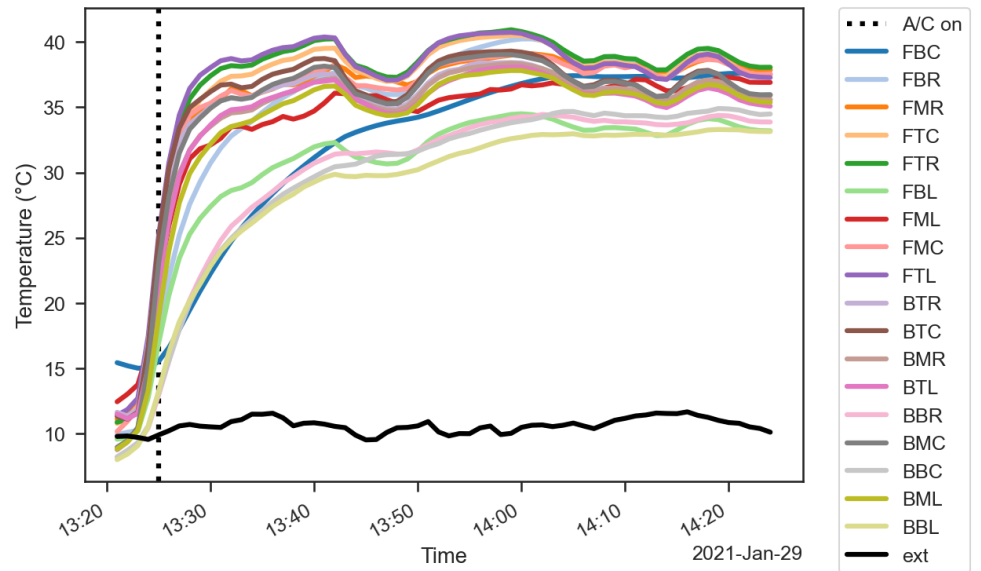


Figure 2. Heating temperature profiles, fresh-air mode.

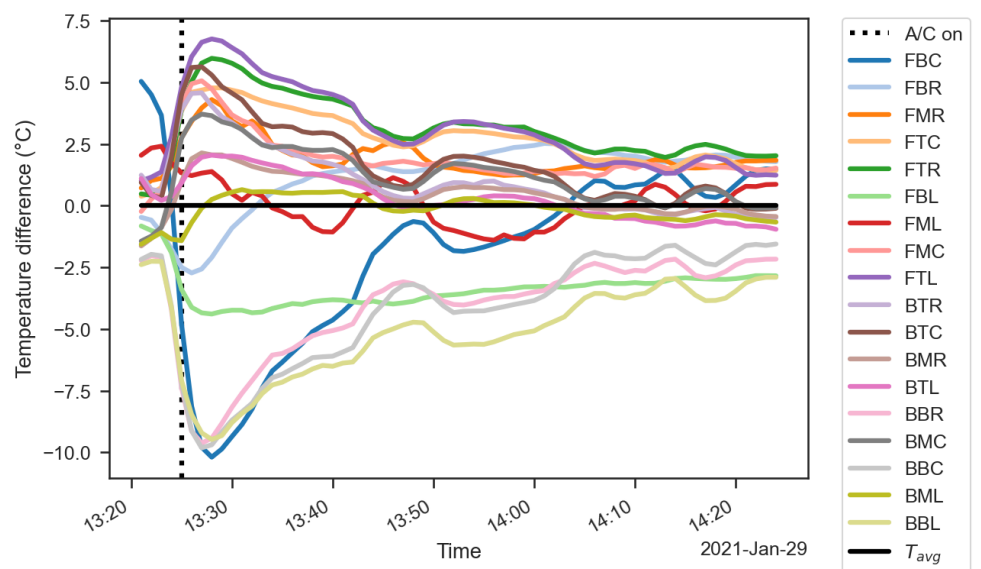


Figure 3. Heating temperature difference profiles, fresh-air mode.

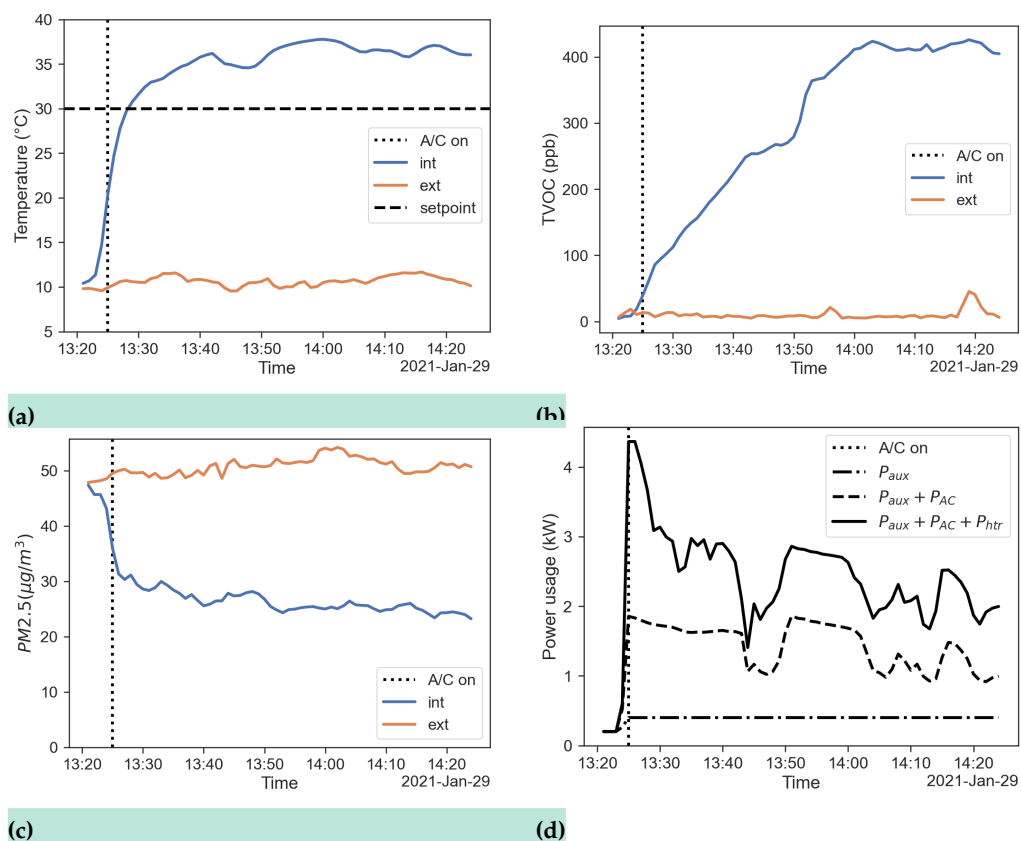


Figure 2. Results regarding the fresh-air mode. (a) Temperature inside (blue) and outside (red) the cabin; (b) TVOC concentration inside (blue) and outside (red) the cabin; (c) PM2.5 concentration inside (blue) and outside (red) the cabin; (d) power usage of the HVAC system.

217 while the HVAC system is working, even with a fresh-air mode. This effect is related
 218 to the presence of sources of VOC inside the vehicle cabin and build up phenomena
 219 during HVAC operation, as expected from the literature [29]. Figure 2(c) displays the
 220 PM2.5 concentration measured inside and outside the cabin in fresh-air mode. Figure
 221 shows that the PM concentrations decrease while the HVAC system is working, due
 222 to the filtering activity of the HVAC filter. This result ties with what is found in the
 223 literature [10]. For the case analysed, a filtration efficiency of about $\eta = 0.5$ for PM2.5
 224 is ascertained. The power usage of the HVAC system, with the contributions of power
 225 used by auxiliary equipment, A/C system and PTC heater recorded by the OBD system
 226 is shown in the stacked line plot in Fig. 2(d).

227 3.1.2. Recirculation configuration

228 Similar considerations can be made for the case with recirculation activated. From
 229 the results shown in Figure 3 it is clear that the time to steady state is close to 20 min;
 230 again the over-temperature issue remains significant. TVOC concentration reached a
 231 value similar to the case without recirculation, but in a longer time with respect to the
 232 fresh-air mode. A possible explanation for this behaviour could rely on the fact the
 233 source of VOCs inside the cabin is compensated by an improved adsorption performance,
 234 as observed by [10]. The PM concentrations decrease to lower values with respect to the
 235 fresh-air mode, as shown in Fig. 3(c). This result shows that the filtration performance is
 236 improved by the recirculation mode. Figure 3(d) shows the power usage of the HVAC
 237 system. The figure shows contributions of auxiliary equipment, A/C system and PTC
 238 heater to the overall power usage.

166 3. Results

167 The measurement system has been characterised both in winter and in summer
168 conditions. In the following sections, two typical conditions for winter and summer
169 have been chosen, to characterise the HVAC system performance in heating and cooling
170 operations respectively. Winter tests have been performed on January 29, 2021, while
171 summer test have been carried out from July 14 to July 15, 2021.

172 3.1. Heating operation

173 Amid winter period, two different test conditions have been investigated, starting
174 from a state of equilibrium with the external environment, obtained maintaining all
175 systems off and all doors opened for 15 minutes. Once the equilibrium was reached,
176 the proper test was performed while maintaining the heater on for 1 hour, the set-point
177 temperature at its maximum of 30 °C, the fan speed at its maximum, all the windows
178 and all the doors closed. During the first test, the recirculation system was off (that
179 means that the air ventilation system was in fresh-air configuration), while during the
180 second test the recirculation system was on.

181 3.1.1. Fresh-air configuration

182 All the experiments confirm that the heating system is capable of reaching a quasi-
183 steady state condition in about 20 min, even though the temperature reached by the air
184 inside the cabin is well over the set-point temperature. Figure 2 shows the readings
185 from all the 18 temperature sensors in the cabin for the case with fresh-air mode with a 3
186 letters naming scheme:

- 187 1. The first letter tells us if we are in the front (F) or in the back (B) of the cabin.
- 188 2. The second letter refers to the location in vertical direction, namely bottom (B),
189 middle (M) and top (T) plane.
- 190 3. The third letter refers to the location in the horizontal direction, namely left (L) or
191 driver, center (C) or right (R) side.

192 Colder spots can be found at feet level of the back seats, moreover this is in disagreement
193 with the studies of Nilsson on equivalent temperature of body segments [20]. In other
194 words, analysing the results of the work that led to the development of the only available
195 standard for comfort evaluation in vehicles (ISO-14505), we can infer that occupants will
196 be likely to accept colder temperatures in upper body parts during winter, while here we
197 are in the opposite situation. Data from position FBC have a different behaviour because
198 it refers to the sensor installed inside the acquisition system box, thus suffering from
199 thermal inertia issues.

200 Defining a temperature difference $\Delta t = t_i - t_{avg}$ where t_i is the temperature
201 in one generic position of the grid, and t_{avg} the mean value of the 18 temperature
202 readings for each timestamp; is possible to obtain Figure 3. It is worth noting that air
203 temperature inside the cabin can reach discrepancies of more than 15 °C in the first
204 minutes of operation, while the Δt values at the end of test is lower and the temperature
205 distribution much more uniform.

206 Figure 4(a) shows the temperature measured inside and outside the cabin keeping
207 the fresh-air mode. In the following air temperature inside the cabin is considered equal
208 to the average of all the sensors on the grid $t_{int} = t_{avg}$.

209 Figure 4(b) reports TVOC concentration measured inside and outside the cabin in
210 fresh-air mode. The system is able to detect a TVOC concentration increase while the
211 HVAC system operates, even with an external air mixing. This behaviour confirms the
212 presence of a source of VOC inside the Leaf's cabin and a build up phenomenon during
213 HVAC operation, as expected from literature [11].

214 Figure 4(c) displays the PM2.5 concentration measured inside and outside the cabin
215 in fresh-air mode. This result ties with what is found in literature [21], the cabin filter is
216 well capable of lowering the PM concentration inside the car with a steady state filtration
217 efficiency of about $\eta = 0.5$.

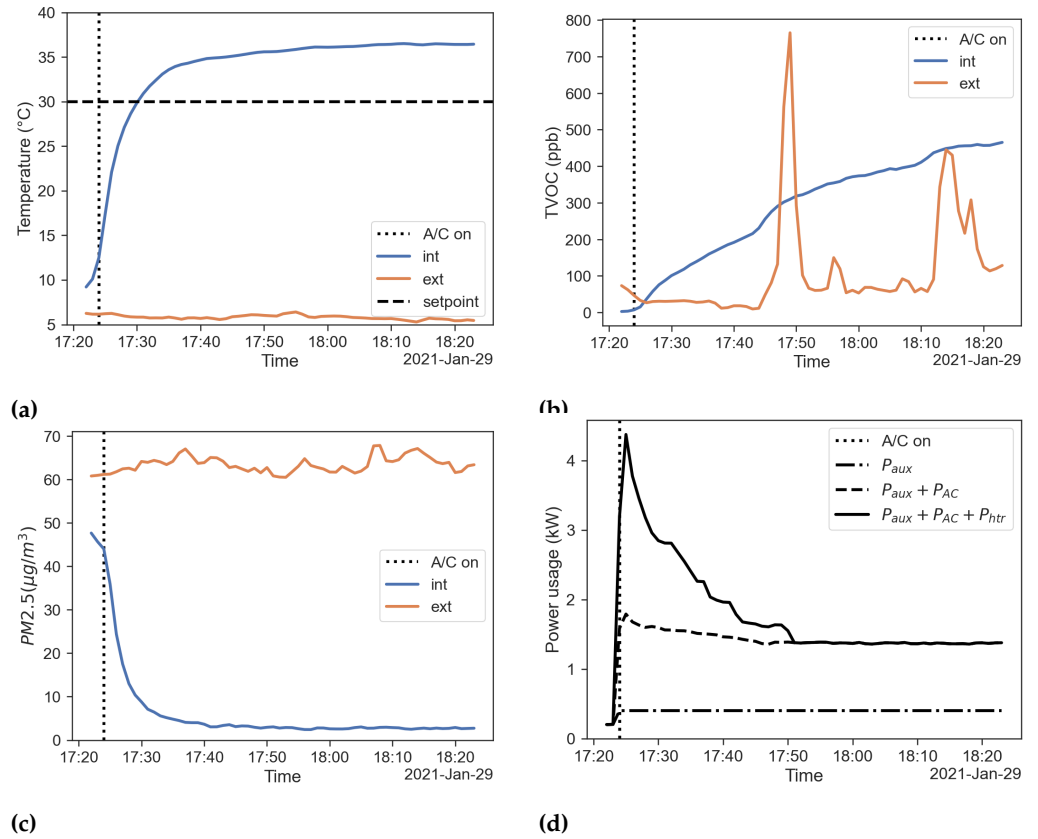


Figure 3. Results regarding the recirculation mode. (a) Temperature inside (blue) and outside (red) the cabin; (b) TVOC concentration inside (blue) and outside (red) the cabin; (c), PM2.5 concentration inside (blue) and outside (red) the cabin; (d) power usage of the HVAC system.

239 3.1.3. Comparison between fresh-air and recirculation mode in winter

The open-field tests conducted in this work have been chosen because representative of the real operating conditions of the vehicle. On the other hand, the experiments have been performed with no control on the environment outside the cabin, with repeatability issues. In order to compare the experiments, the following dimensionless temperature is defined:

$$240 \quad t^* = \frac{t_{int} - t_{ext}}{t_{set} - t_{ext}} \quad (1)$$

241 where t^* is the dimensionless temperature, t_{int} is the air temperature measured inside
 242 the cabin, t_{ext} is the air temperature measured outside the cabin and t_{set} is the set-point
 243 temperature. It is worth to underline that when $t_{int} = t_{ext}$, dimensionless temperature t^*
 244 is equal to 0, while when $t_{int} = t_{set}$, then t^* is equal to 1. These two key points represent
 245 two relevant physical states, equilibrium with the external environment and fulfilment
 246 of the set-point request, respectively. Figure 4(a) shows a comparison between the
 247 dimensionless temperatures obtained for the two experiments. It is noticeable that the
 248 dimensionless temperature obtained without recirculation is always higher than the one
 249 obtained in the case of recirculation mode, thus suggesting that the over-temperature
 250 issue is more significant in this case. In addition, the set-point is reached faster during the fresh-air mode than during the recirculation mode.

The filtration efficiency of the vehicle can be defined using a black box approach, where the vehicle cabin is considered as a system with an unknown filtration capacity, while inlet (external) and outlet (internal) concentrations are known. The filtration efficiency is then defined by

$$\eta = 1 - \frac{C_{int}}{C_{ext}} \quad (2)$$

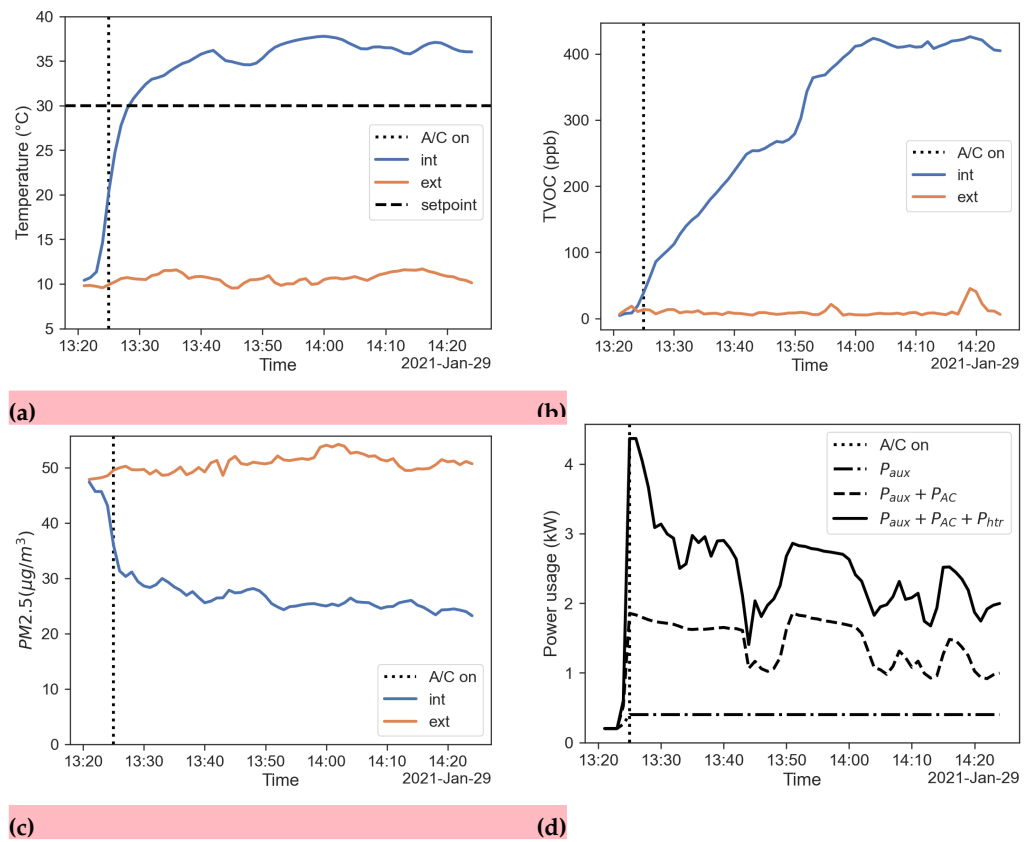


Figure 4. Results regarding the fresh-air mode. (a) Temperature inside (blue) and outside (red) the cabin; (b) TVOC concentration inside (blue) and outside (red) the cabin; (c) PM2.5 concentration inside (blue) and outside (red) the cabin; (d) power usage of the HVAC system.

218 A first example of what kind of data can be acquired with the OBD system is given
 219 in figure 4(d), where stacked plots of the power usage of the HVAC system are shown.

220 3.1.2. Recirculation configuration

221 Figure 5 shows the readings from all the 18 temperature sensors in the cabin for the
 222 case with recirculation mode. Air temperature inside the cabin shows slightly higher
 223 discrepancies with respect to the previous case, colder spots can be found again at feet
 224 level of the back seats. Signal from the FBC sensor shows similar responsiveness issues
 225 as for the case without recirculation. Higher temperature gradients in the startup phase
 226 are evident from Figure 6, while a smoother profile is reached at the end of test.

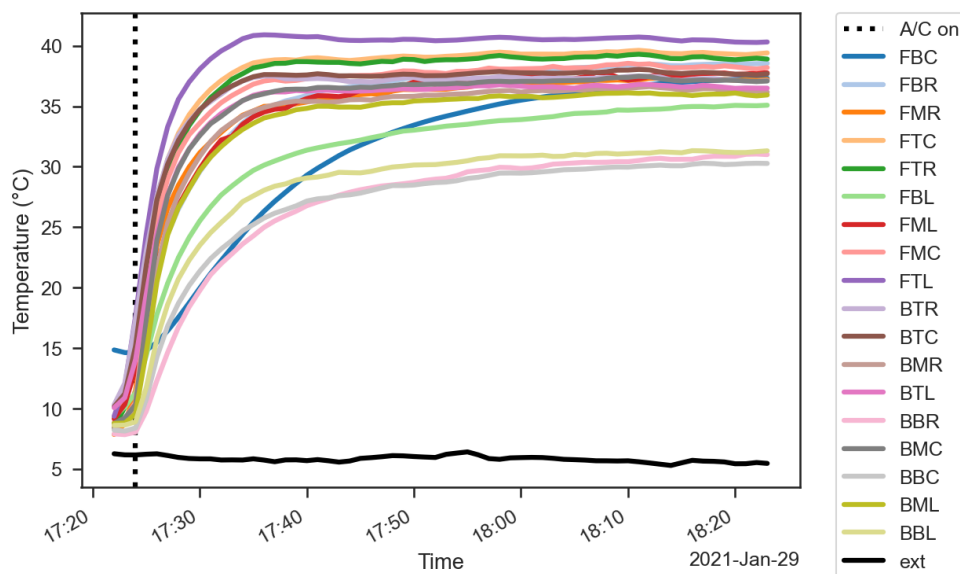


Figure 5. Heating temperature profiles, recirculation mode.

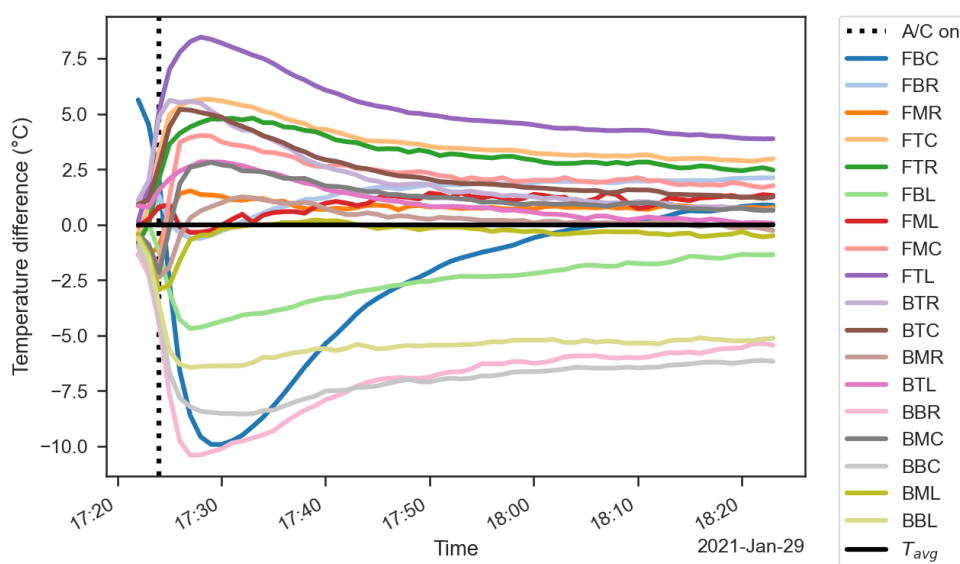


Figure 6. Heating temperature difference profiles, recirculation mode.

227 Similar considerations can be made for the case with recirculation activated. From
 228 the results shown in Figure 7 it is clear that the time to steady state is close to 20 min;
 229 again the over-temperature issue remains significant. TVOC concentration reached a
 230 similar value as the case without recirculation, but slower. A possible explanation for

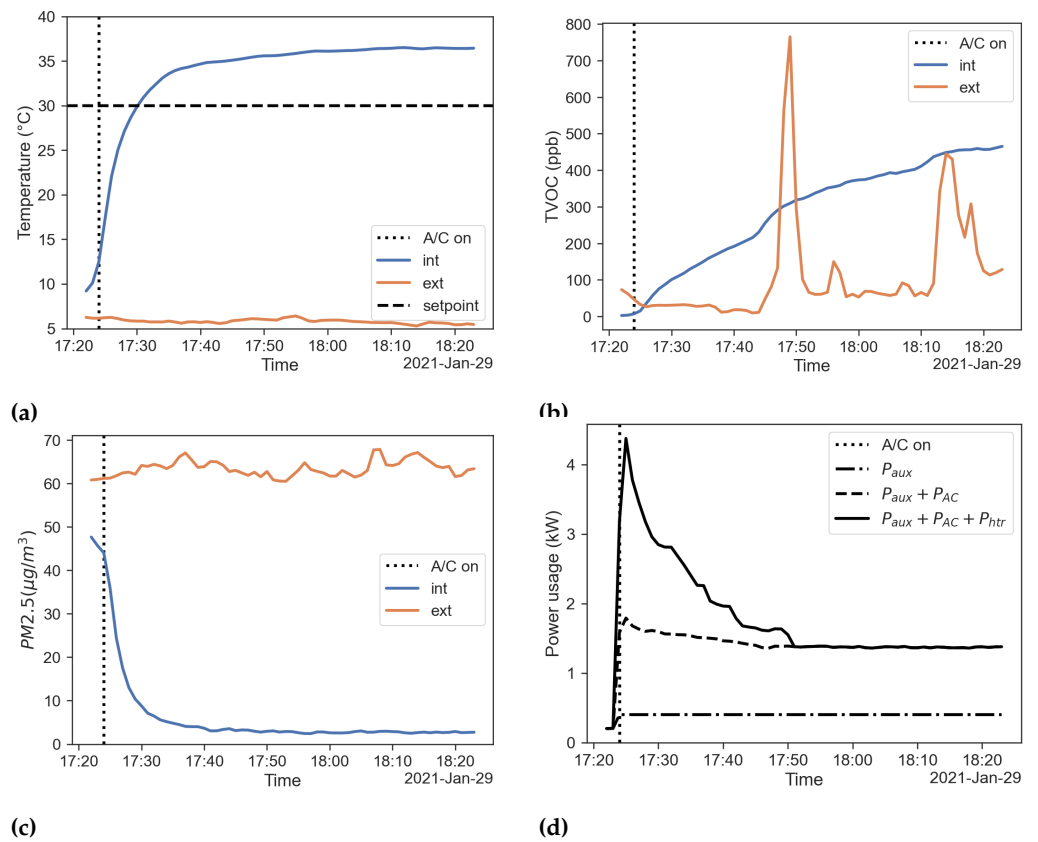


Figure 7. Results regarding the recirculation mode. (a) Temperature inside (blue) and outside (red) the cabin; (b) TVOC concentration inside (blue) and outside (red) the cabin; (c), PM2.5 concentration inside (blue) and outside (red) the cabin; (d) power usage of the HVAC system.

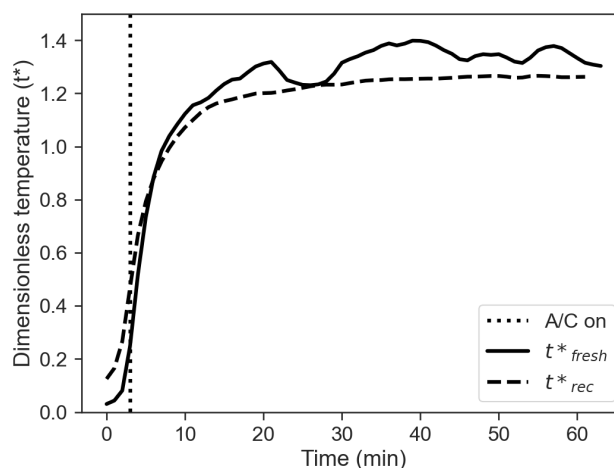
231 this behaviour could rely on the fact that even without fresh air mixing, the source
 232 of VOCs inside the cabin is compensated by an improved adsorption performance in
 233 recirculation mode. This happens mostly if the breakthrough time is not yet reached [21].
 234 As for the PM values, it is pretty clear from Fig. 7(c) how the filtration performance is
 235 improved by the recirculation mode.

236 3.1.3. Comparison between fresh-air and recirculation mode in winter

The open field tests conducted in this work share similarities with the real operating conditions of the vehicle. On the other hand, the experiments have been performed with no control on the environment outside the cabin, with repeatability issues. In order to compare the experiments, the following dimensionless temperature is defined:

$$t^* = \frac{t_{int} - t_{ext}}{t_{set} - t_{ext}} \quad (1)$$

237 where t^* is the dimensionless temperature, t_{int} is the air temperature measured inside
 238 the cabin, t_{ext} is the air temperature measured outside the cabin and t_{set} is the set-point
 239 temperature. It is worth to underline that when $t_{int} = t_{ext}$, dimensionless temperature
 240 t^* is equal to 0, while when $t_{int} = t_{set}$, then t^* is equal to 1. These two key points
 241 represent two relevant physical states, equilibrium with the external environment and
 242 fulfilment of the set-point request respectively. Figure 8 shows a comparison between the
 dimensionless temperatures obtained for the two experiments. It is noticeable that the



243 **Figure 8.** Dimensionless temperature profiles, comparison between fresh-air mode (solid line) and
 244 recirculation (dashed line) mode.

245 dimensionless temperature obtained without recirculation is always higher than the one
 246 obtained in the case of recirculation mode, thus suggesting that the over-temperature
 247 issue is more significant in this case. In addition, the set-point is reached faster during
 the fresh-air mode than during the recirculation mode.

The filtration efficiency of the vehicle can be defined using a black box approach, where the vehicle cabin is considered as a system with an unknown filtration capacity, while inlet (external) and outlet (internal) concentrations are known:

$$\eta = 1 - \frac{C_{int}}{C_{ext}} \quad (2)$$

248 Figure 9 shows a comparison between the two cases. The PM filtration efficiency
 249 with recirculation mode is almost double than the one with the fresh-air mode. It is
 250 also noticeable that the filtration efficiency does never reach the ideal value of $\eta = 1$,
 251 suggesting that infiltration rate not equal to zero occur even if the vehicle is parked.

252 An alternative method to get insights about IAQ of a vehicle cabin relies on a time
 253 integrated inside/outside approach [3]. The associated index, named Cabin Air Quality
 254 Index (CAQI) is defined as follows:

$$CAQI = \frac{\int_{t_i}^{t_f} C_{int}(t) dt}{\int_{t_i}^{t_f} C_{ext}(t) dt} \quad (3)$$

255 Results based on this index for PM_{2.5} and TVOC are given in Figures 10 and 11.

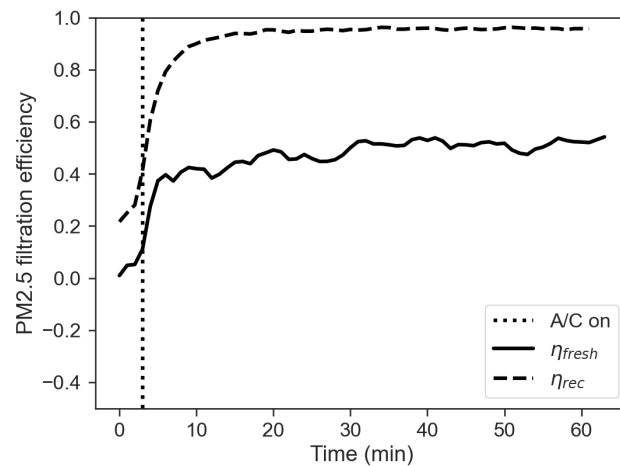


Figure 9. Filtration efficiency, comparison between fresh-air (solid line) and recirculation (dashed line) mode.

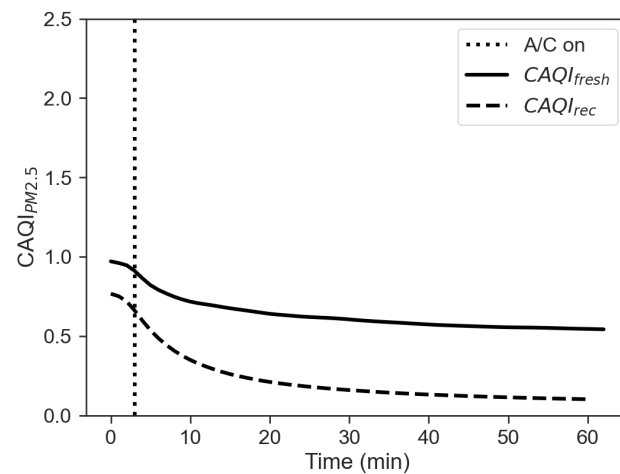
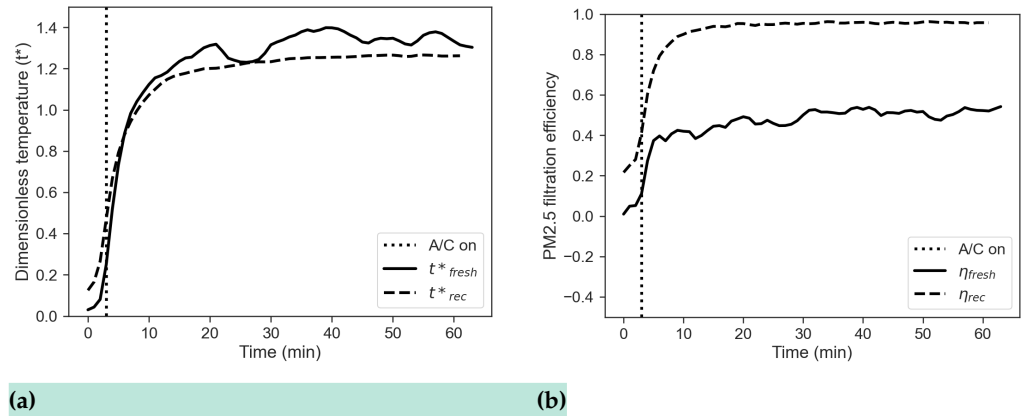


Figure 10. CAQI for PM_{2.5}.

Figure 12 shows the comparison between the cumulative energy consumption in the two cases of recirculation on and off, calculated as the approximate cumulative integral of $P_{tot} = P_{aux} + P_{AC} + P_{Htr}$ via the trapezoidal method in order to integrate numeric data rather than a functional expression:

$$E = \int_{t_i}^{t_f} P_{tot}(t) dt \approx \frac{t_f - t_i}{2N} \sum_{n=1}^N (P_{tot}(t_n) + P_{tot}(t_{n+1})) \quad (4)$$

256 where t_i is the start time, t_f the final time and $N+1$ the number of samples available
 257 (equally spaced). The total energy consumption obtained in the recirculation mode on
 258 is about 3/4 of the value obtained for the fresh-air mode. This result can explain what
 259 is shown in figures 4(d) and 7(d). These figures show that the power usage from the



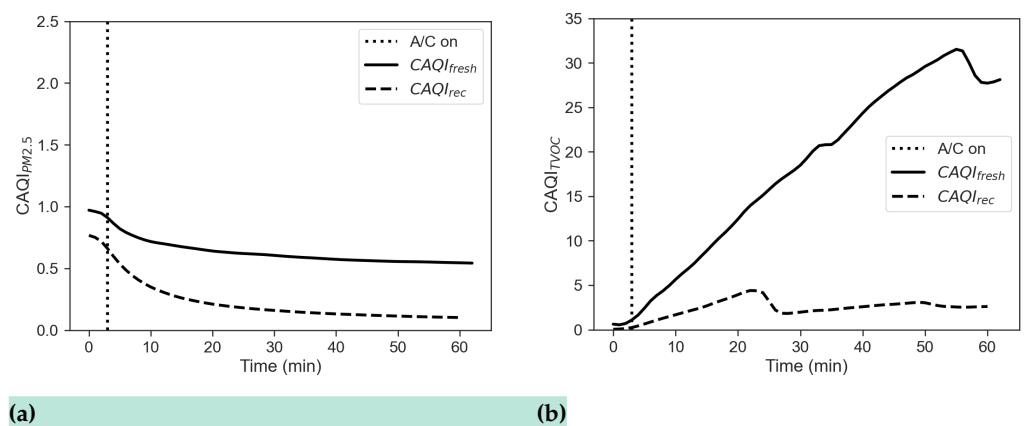
(a) **(b)**
Figure 4. (a) Dimensionless temperature profiles, comparison between fresh-air (solid line) and recirculation (dashed line) mode. (b) Filtration efficiency, comparison between fresh-air (solid line) and recirculation mode (dashed line).

251 where C_{int} and C_{ext} are the internal and external concentrations, respectively. Figure 4(b)
 252 shows a comparison between the PM filtration efficiency obtained in the two regimes.
 253 The figure shows that PM filtration efficiency with recirculation mode is almost double
 254 than the one obtained with the fresh-air mode. It is also noticeable that the filtration
 255 efficiency does never reach the ideal value of $\eta = 1$, suggesting that infiltration rate not
 256 equal to zero occur even if the vehicle is parked.

An alternative method to get insights about IAQ of a vehicle cabin relies on a time integrated inside/outside approach proposed in [13]. The associated index, named Cabin Air Quality Index (CAQI) is defined as follows:

$$CAQI = \frac{\int_{t_i}^{t_f} C_{int}(t) dt}{\int_{t_i}^{t_f} C_{ext}(t) dt} \quad (3)$$

where C_{int} is the internal concentration, C_{ext} is the external concentration, t_i is the start time and t_f is the stop time. Results based on this index for PM2.5 and TVOC are given in Figure 5. The figure shows that the CAQI indexes for PM2.5 and VOC obtained for



(a) **(b)**
Figure 5. (a) CAQI for PM2.5 and (b) CAQI for TVOC.

the fresh-air mode are much greater than the one obtained for the recirculation mode. Figure 6 shows the comparison between the cumulative energy consumption in the two cases of recirculation on and off, calculated as the approximate cumulative integral of

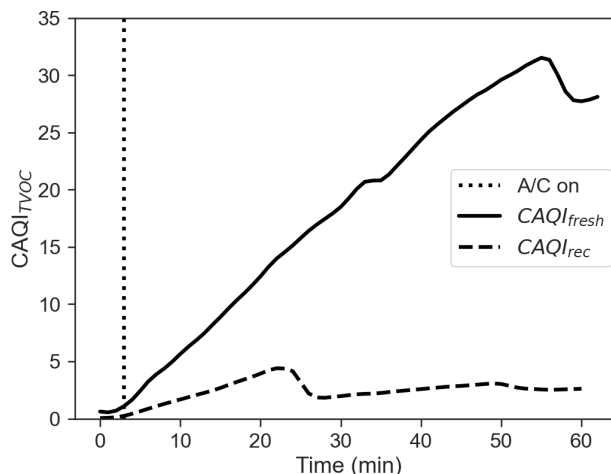


Figure 11. CAQI for TVOC.

260 HVAC system is similar for the two modes in the first minutes of operation. However,
 261 when the effects of recirculation become prevalent, the values of the HVAC power usage
 262 related to the two modes differ. Infact, while P_{tot} peaks at more than 4 kW in the first
 263 minutes of operation in both modes, it varies significantly towards the end of the test.

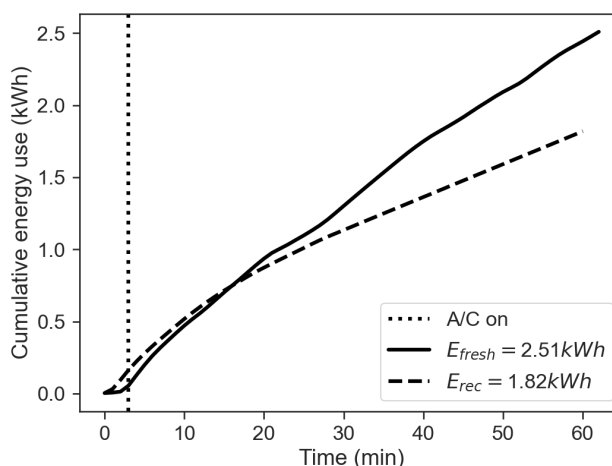


Figure 12. Cumulative energy use, comparison between fresh-air (solid line) and recirculation (dashed line) mode.

264 3.2. Cooling operation

265 Two different test conditions have been investigated starting from a state of equi-
 266 librium with the external environment, obtained maintaining all systems off and all
 267 doors opened for 15 minutes. Once the equilibrium was reached, the proper test was
 268 performed while maintaining the A/C on for 1 hour, the set-point temperature at its
 269 minimum of 16 °C, the fan speed at its maximum, all the windows and all the doors
 270 closed. During the first test, the recirculation system was off (that means that the air
 271 ventilation system was in fresh-air configuration), while during the second test the
 272 recirculation system was on.

273 3.2.1. Recirculation mode off

274 All the experiments confirm that the cooling system is not capable of reaching a
 275 quasi-steady state condition in about 60 min, textit*i.e.* the temperature reached by the
 276 air inside the cabin is far from the set-point temperature value. Figure 13 shows the

$P_{tot} = P_{aux} + P_{AC} + P_{Htr}$ via the trapezoidal method, in order to integrate numeric data rather than a functional expression:

$$E = \int_{t_i}^{t_f} P_{tot}(t) dt \approx \frac{t_f - t_i}{2N} \sum_{n=1}^N (P_{tot}(t_n) + P_{tot}(t_{n+1})) \quad (4)$$

where t_i is the start time, t_f the final time and $N+1$ the number of samples available (equally spaced). The total energy consumption obtained in the recirculation mode is about 3/4 of the value obtained for in fresh-air mode. This result can explain what is shown in figures 2(d) and 3(d). These figures show that the power usage from the HVAC system is similar for the two modes in the first minutes of operation. However, when the effects of recirculation become prevalent, the values of the HVAC power usage related to the two modes differ considerably. In fact, while P_{tot} peaks at more than 4 kW in the first minutes of operation in both modes, it varies significantly towards the end of the test.

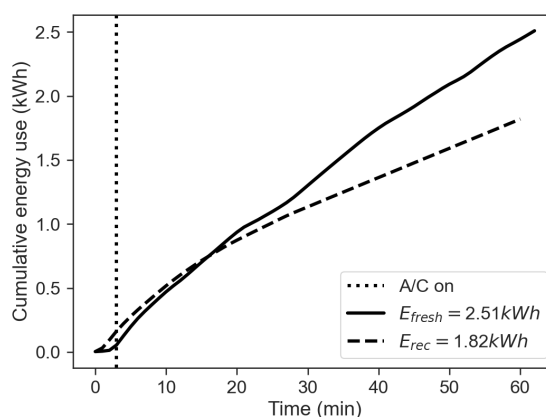


Figure 6. Cumulative energy use, comparison between fresh-air (solid line) and recirculation (dashed line) mode.

3.2. Measurements during cooling operation

Two different test conditions have been investigated starting from a state of equilibrium with the external environment, obtained maintaining all systems off and all doors opened for 15 minutes. Once the equilibrium was reached, the proper test was performed while maintaining the A/C on for 1 hour, the set-point temperature at its minimum of 16 °C, the fan speed at its maximum (position 7), all windows and all doors closed. During the first test, the recirculation system was off (that means that the air ventilation system was in fresh-air configuration), while during the second test the recirculation system was on.

3.2.1. Fresh-air configuration

All the experiments confirm that the cooling system is not capable of reaching a quasi-steady state condition in about 60 min, *i.e.* the temperature reached by the air inside the cabin is far from the set-point temperature value.

Figure 7(a) shows the temperature measured inside and outside the cabin keeping the fresh-air mode. Like for the winter operation, the air temperature inside the cabin is calculated as the mean value of the 18 temperature readings for each timestamp.

Figure 7(b) shows TVOC measured inside and outside the cabin in fresh-air mode. The figure reports that the TVOC concentration is higher than that of the external air at the beginning, but decreases while the HVAC system operates. The lowest concentration is reached, despite the fluctuation on the outside. This behaviour can be explained with a drop of temperature inside the cabin combined with fresh-air mixing, thus reducing the emission from the internal sources.

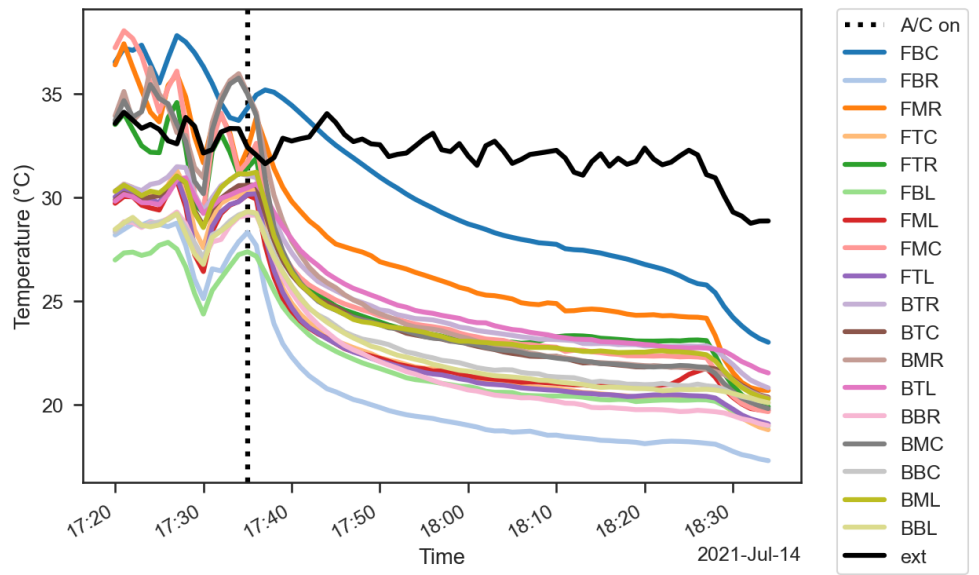


Figure 13. Cooling temperature profiles, fresh-air mode.

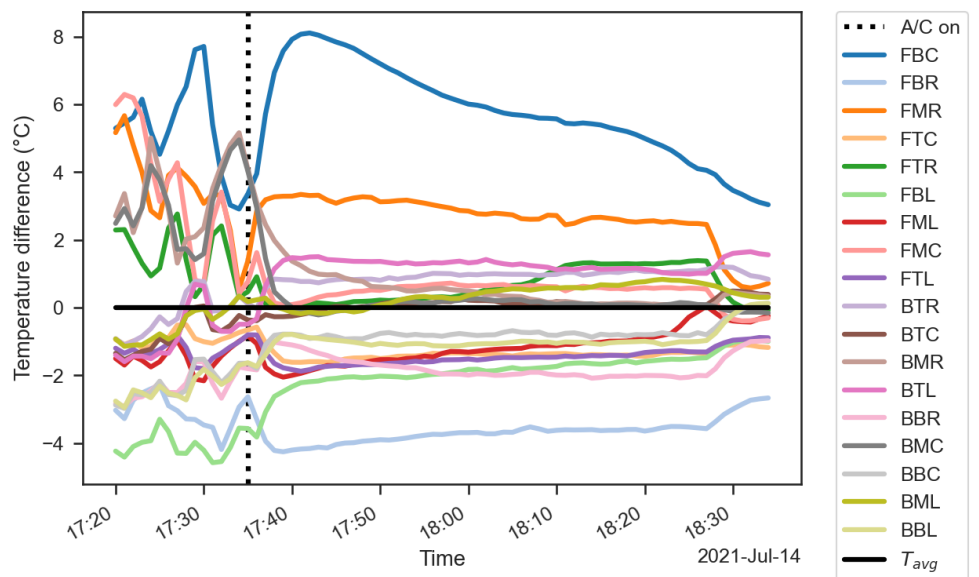


Figure 14. Cooling temperature difference profiles, fresh-air mode.

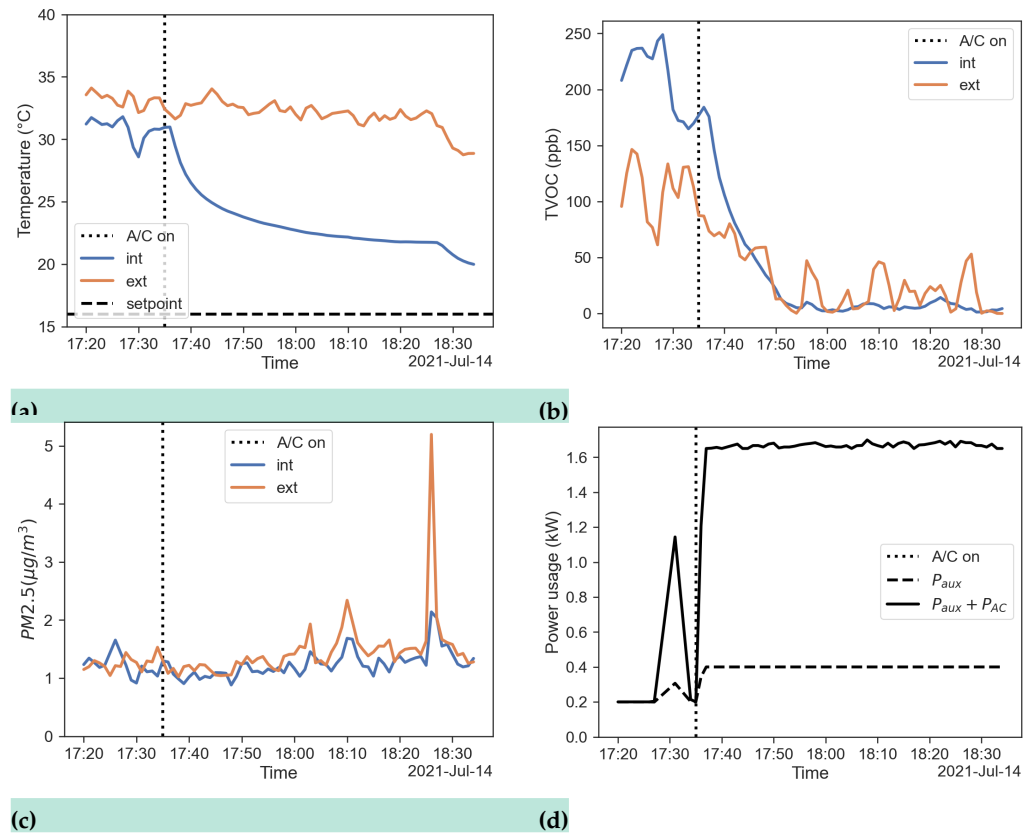


Figure 7. Results regarding the fresh-air mode. (a) Temperature inside (blue) and outside (red) the cabin; (b) TVOC concentration inside (blue) and outside (red) the cabin; (c) PM_{2.5} concentration inside (blue) and outside (red) the cabin; (d) power usage of the HVAC system.

287 Figure 7(c) reports plots of the PM_{2.5} concentration measured inside and outside
 288 the cabin in fresh-air configuration. This result appears to be in contrast with the results
 289 shown by [10], *i.e.* the cabin filter is not able to lower the PM concentration inside the
 290 car with a steady state filtration efficiency $\eta = 0$ to 0.2. Here we need to consider that
 291 the value of PM_{2.5} concentrations measured were extremely low and under the sensor
 292 precision for that particle size range ($\pm 10 \mu\text{g}/\text{m}^3$).

293 Figure 7(d) shows the power usage of the HVAC system. The figure shows the
 294 contributions of power used by auxiliary equipment and A/C system; with PTC heater
 295 power being indeed equal to zero in cooling operation.

296 3.2.2. Recirculation configuration

297 As for the previous case with recirculation activated, time to steady state is close
 298 to 20 min of operation, while the over-temperature issue is still significant. TVOC
 299 concentration shows a different trend. Despite external concentration peaks at the end of
 300 the test, the internal one remains quite low. As for PM values, they follow a completely
 301 different trend, it is pretty clear from Fig. 8(c) how the filtration performance is improved
 302 by the recirculation mode, even with absolute values well within the precision range as
 303 is the previous test. Figure 8(d) shows the power usage of the HVAC system, with the
 304 contributions of power used by auxiliary equipment and A/C system recorded by the
 305 OBD system.

306 3.2.3. Comparison between fresh-air and recirculation modes in summer

307 Experiments in cooling as well as heating mode have been performed in real parking
 308 conditions with no control on the environment outside the cabin, repeatability issues are
 309 worsened by the increased contribution of solar load in summer. In order to compare the

277 readings from all the 18 temperature sensors in the cabin for the case with fresh-air mode
 278 with the same naming scheme introduced in the previous section.

279 Temperature discrepancies in the cabin can approach 12 °C; warmer spots can be
 280 found at top and middle locations, while bottom zone is generally colder (Fig. 14). To
 281 a certain extent, this is in agreement with a stratification of cabin air during operation,
 282 despite the vents working at full power. Looking at "Light summer" Comfort Zones
 283 defined by [20], we can infer that occupants will be likely to accept warmer temperatures
 284 in lower body parts during summer, while this result goes in the opposite direction.
 285 Self heating and thermal inertia issue of the sensor positioned at FBC position are still
 286 evident.

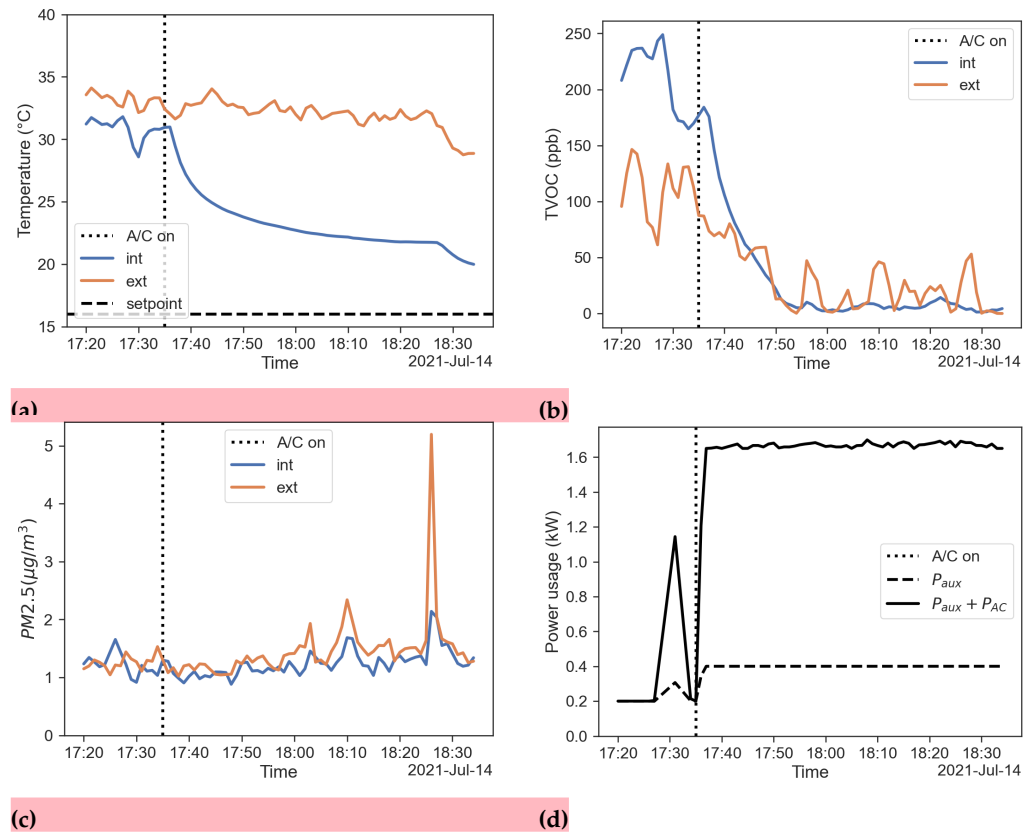


Figure 15. Results regarding the fresh-air mode. (a) Temperature inside (blue) and outside (red) the cabin; (b) TVOC concentration inside (blue) and outside (red) the cabin; (c) PM2.5 concentration inside (blue) and outside (red) the cabin; (d) power usage of the HVAC system.

287 Figure 15(a) shows the temperature measured inside and outside the cabin keeping
 288 the fresh-air mode. Like for the winter operation, the air temperature inside the cabin is
 289 calculated as the mean value of the 18 temperature readings for each timestamp.

290 Figure 15(b) shows TVOC measured inside and outside the cabin during the fresh-
 291 air mode. The figure reports that the TVOC concentration is higher than that of the
 292 external air at the beginning, but decreases while the HVAC system operates. The lowest
 293 concentration is reached, despite the fluctuation on the outside. This behaviour can be
 294 explained with a drop of temperature inside the cabin combined with fresh-air mixing.

295 Figure 15(c) plots the PM2.5 concentration measured inside and outside the cabin
 296 in fresh-air configuration. This result appears to be in contrast with the results shown by
 297 [21], *i.e.* the cabin filter is not able to lower the PM concentration inside the car with a
 298 steady state filtration efficiency $\eta = 0$ to 0.2. Here we need to consider that the value of
 299 PM2.5 concentrations measured were very low and under the sensor precision for that
 300 particle size range ($\pm 10 \mu\text{g}/\text{m}^3$).

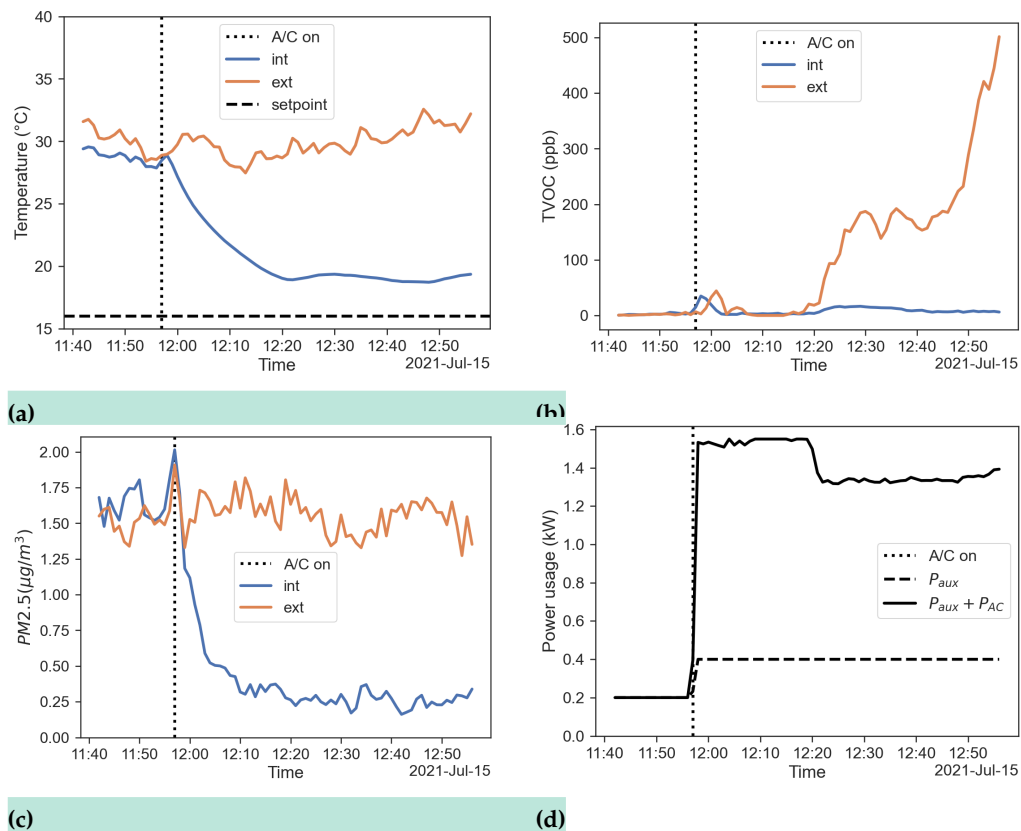


Figure 8. Results regarding the recirculation mode. (a) Temperature inside (blue) and outside (red) the cabin; (b) TVOC concentration inside (blue) and outside (red) the cabin; (c) PM2.5 concentration inside (blue) and outside (red) the cabin; (d) power usage of the HVAC system.

310 experiments, a temperature adimensionalisation is performed according to equation
 311 1. Figure 9(a) shows a comparison between the dimensionless temperatures obtained
 312 for the two experiments. It is noticeable that the value of dimensionless temperature
 313 obtained with recirculation is always higher than the one obtained in the fresh-air case,
 314 thus suggesting that the cabin approaches better the set-pot in the first case. The filtration
 315 efficiency of the vehicle can be defined again using a black box approach, where the
 316 vehicle cabin is considered as a system with an unknown filtration capacity, while inlet
 317 (external) and outlet (internal) concentrations are known, according to equation 2. Figure
 318 9(b) shows a comparison between the two cases. The PM filtration efficiency with
 319 recirculation mode is well over the one with the fresh-air mode. It is also noticeable
 320 that as for the winter case the filtration efficiency does never reach the ideal value of
 321 $\eta = 1$, but it is even lower indeed. This trend can be explained with η being function
 322 of particle size[10], but also of particle concentration itself. As shown for the winter
 323 case, another way to investigate cabin performance on airborne pollutants is provided
 324 by equation 3. Figure 10 reports the CAQI trend for PM2.5 and TVOC in fresh-air and
 325 recirculation, the latter being less prone to build up of pollutants during operation.
 326 Figure 11 shows the comparison between the cumulative energy consumption in the two
 327 cases of recirculation on and off, calculated as the approximate cumulative integral of
 328 $P_{tot} = P_{aux} + P_{AC}$ via the trapezoidal method as done in the winter case with equation
 329 4. The total energy consumption obtained in the recirculation mode on is about 4/5
 330 of the value obtained for the fresh-air mode. This result can explain what is shown in
 331 figures 7(d) and 8(d). These figures show that the power usage from the HVAC system is
 332 similar for the two modes in the first minutes of operation. However, when the effects of
 333 recirculation become prevalent, the HVAC power usage related to this mode decreases
 334 after about 20 min, even though the difference is less prominent than in winter operation.

301 3.2.2. Recirculation mode

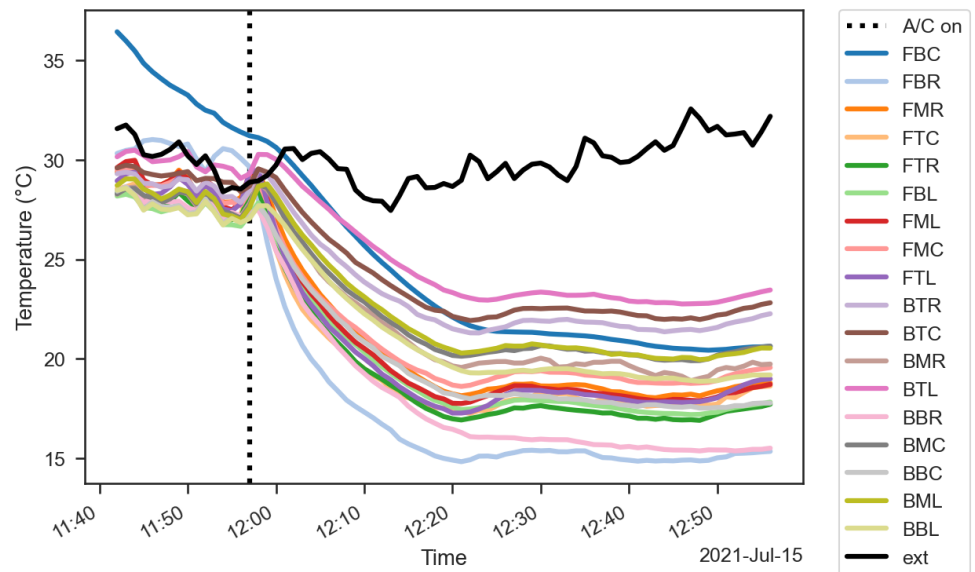


Figure 16. Cooling temperature profiles, recirculation mode.

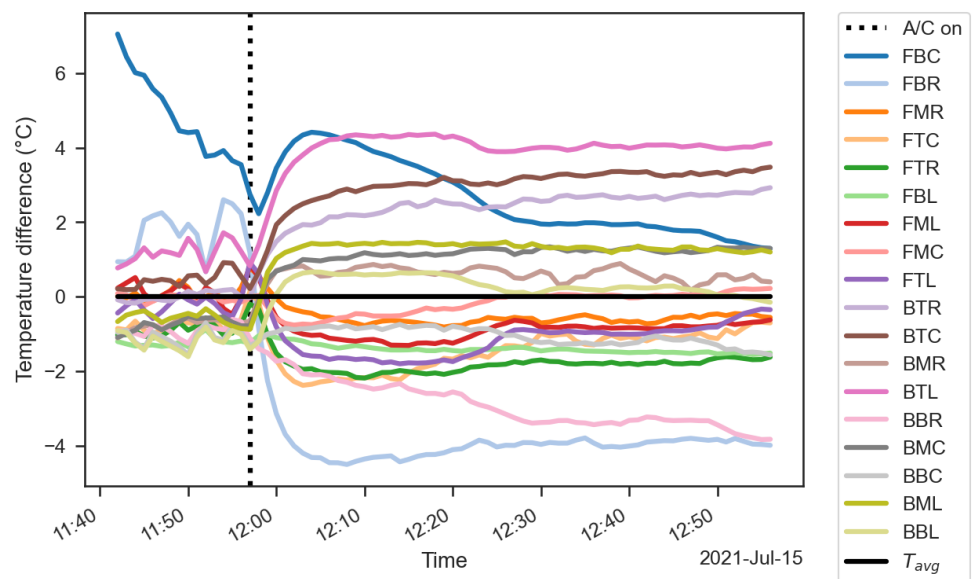


Figure 17. Cooling temperature difference profiles, recirculation mode.

302 Figure 16 shows the readings from all the 18 temperature sensors in the cabin for the
 303 case with recirculation mode. Air temperature stratification with respect to the vertical
 304 axis is again considerable, colder spots can be found at feet level of the back seats. The
 305 main difference with the fresh-air case is that bottom right location are well capable of
 306 reaching the set-point temperature.

307 As for the previous case with recirculation activated, time to steady state is close
 308 to 20 min of operation, while the over-temperature issue is still significant. TVOC
 309 concentration show a totally different trend. Despite external concentration peaks
 310 at the end of the test, the internal one remains quite low. As for PM values, they
 311 follow a completely different trend, it is pretty clear from Fig. 18(c) how the filtration
 312 performance is improved by the recirculation mode, even with absolute values well
 313 within the precision range as is the previous test.

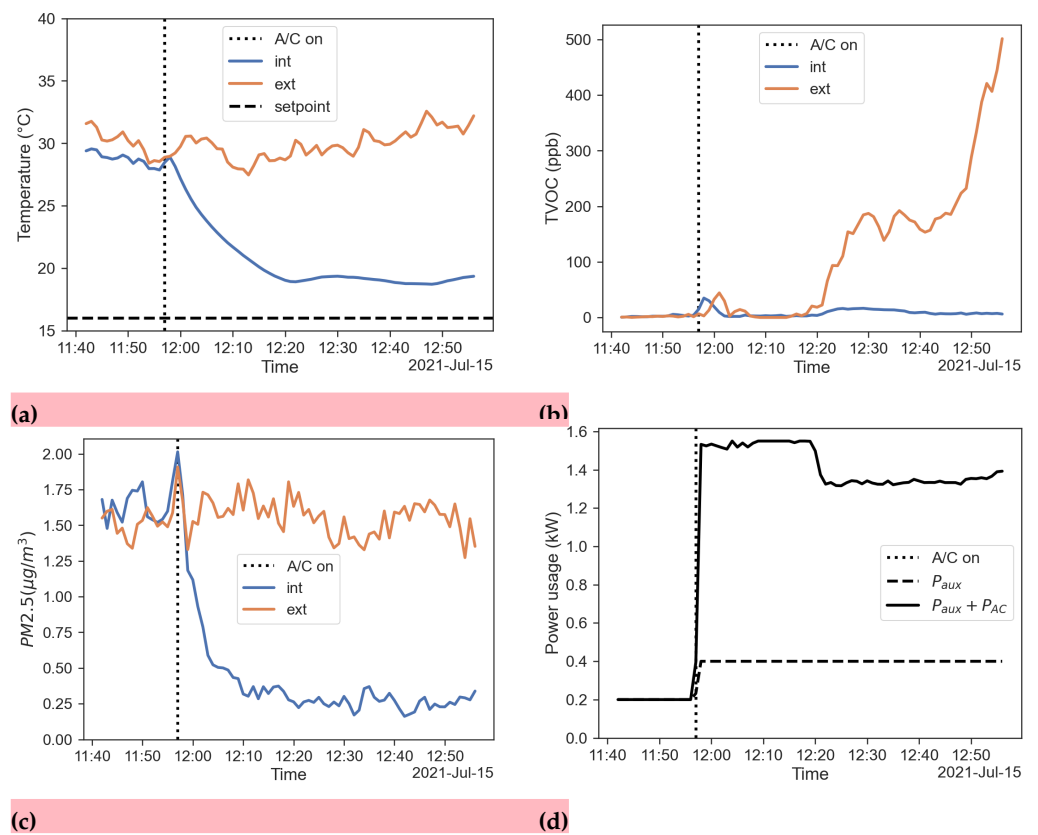


Figure 18. Results regarding the recirculation mode. (a) Temperature inside (blue) and outside (red) the cabin; (b) TVOC concentration inside (blue) and outside (red) the cabin; (c), PM2.5 concentration inside (blue) and outside (red) the cabin; (d) power usage of the HVAC system.

3.2.3. Comparison between fresh-air and recirculation modes in summer

Experiments in cooling as well as heating mode have been performed in real parking conditions with no control on the environment outside the cabin, repeatability issues are worsened by the increased contribution of solar load in summer. In order to compare the experiments, a temperature adimensionalisation is performed according to equation 1. Figure 19 shows a comparison between the dimensionless temperatures obtained for the two experiments. It is noticeable that the value of dimensionless temperature

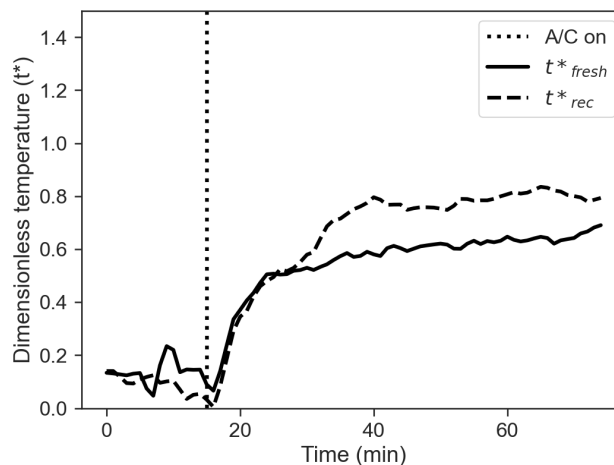


Figure 19. Dimensionless temperature profiles, comparison between fresh-air (solid line) and recirculation (dashed line) mode.

obtained with recirculation is always higher than the one obtained in the fresh-air case, thus suggesting that the cabin approaches better the set-point in the first case.

The filtration efficiency of the vehicle can be defined again using a black box approach, where the vehicle cabin is considered as a system with an unknown filtration capacity, while inlet (external) and outlet (internal) concentrations are known, according to equation 2. Figure 20 shows a comparison between the two cases. The PM filtration efficiency with recirculation mode is well over the one with the fresh-air mode. It is also noticeable that as for the winter case the filtration efficiency does never reach the ideal value of $\eta = 1$, but it is even lower indeed. This trend can be explained with η being function of particle size[21], but also of particle concentration itself.

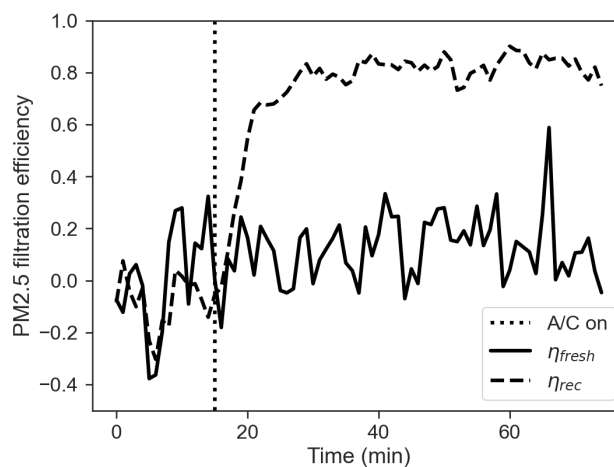


Figure 20. Filtration efficiency, comparison between fresh-air mode (solid line) and recirculation (dashed line) mode.

As shown for the winter case, another way to investigate cabin performance on airborne pollutants is provided by equation 3. Figures 21 and 22 report the CAQI trend

333 for PM_{2.5} and TVOC in fresh-air and recirculation, the latter being less prone to build
 334 up of pollutants during operation.

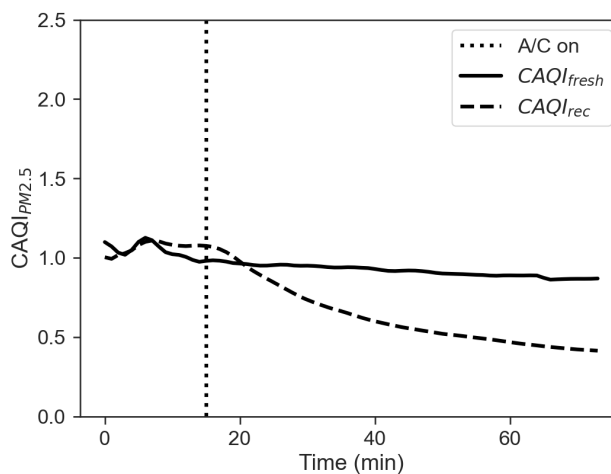


Figure 21. CAQI for PM_{2.5}.

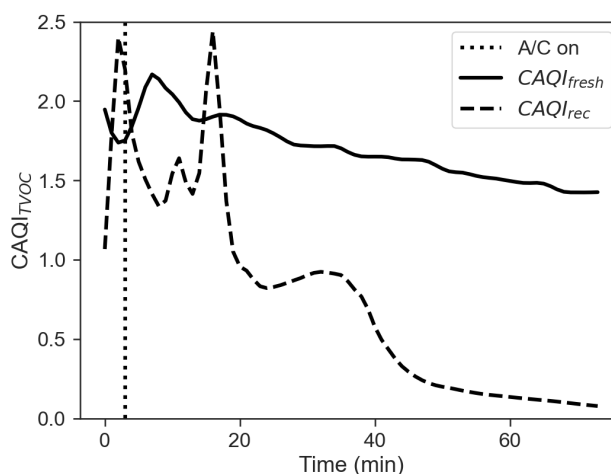


Figure 22. CAQI for TVOC.

335 Figure 23 shows the comparison between the cumulative energy consumption in
 336 the two cases of recirculation on and off, calculated as the approximate cumulative
 337 integral of $P_{tot} = P_{aux} + P_{AC}$ via the trapezoidal method as done in the winter case with
 338 equation 4. The total energy consumption obtained in the recirculation mode on is about
 339 4/5 of the value obtained for the fresh-air mode. This result can explain what is shown in
 340 figures 15(d) and 18(d). This figures show that the power usage from the HVAC system
 341 is similar for the two modes in the first minutes of operation. However, when the effects
 342 of recirculation become prevalent, the HVAC power usage related to this mode becomes
 343 lower after about 20 min, even though the difference is less prominent than in the winter
 344 operation.

345 3.3. Effect of filter conditions on filtration performance

346 In this section we report some results regarding the filtration performances of the
 347 Leaf cabin filter (Figure 24). In detail we performed two tests in summer operating
 348 conditions manipulating the filter. First, we performed the experiment without the filter.
 349 Then, a second experiment was performed after installing a new brand filter. Figure
 350 24(a) shows that the presence of the filter has an effect of filtration efficiency, lowering
 351 its value from 80 % to 60 %. The figure shows that even without a filter the recirculation

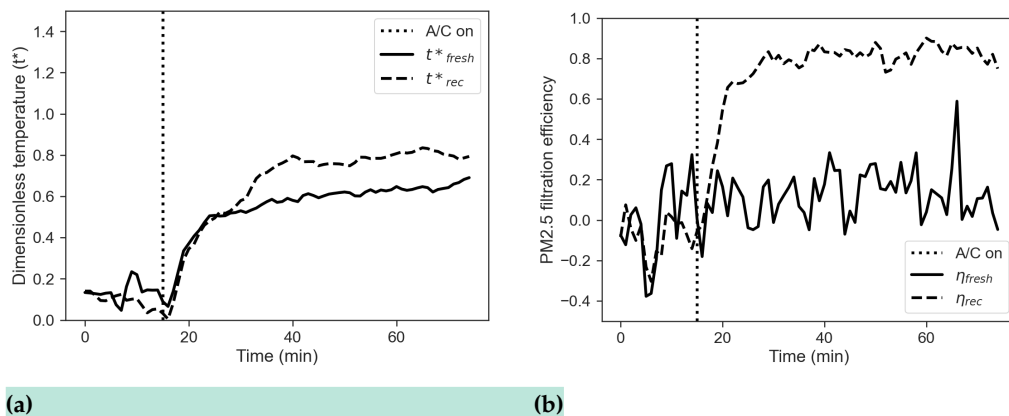


Figure 9. (a) Dimensionless temperature profiles, comparison between fresh-air (solid line) and recirculation (dashed line) mode. (b) Filtration efficiency, comparison between fresh-air (solid line) and recirculation mode (dashed line).

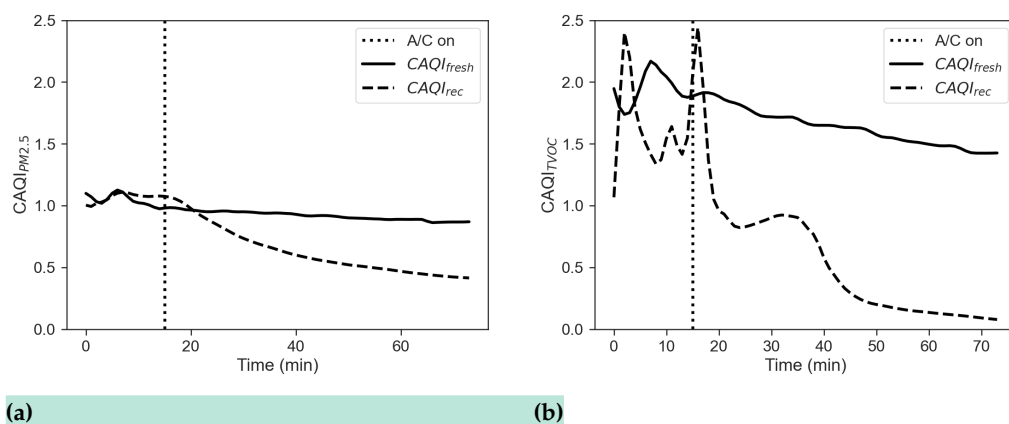


Figure 10. (a) CAQI for PM2.5 and (b) CAQI for TVOC.

3.3. Effect of filter conditions on filtration performance

In this section we report some results regarding the filtration performances of the Leaf cabin filter (Figure 12). In detail we performed two tests in summer operating conditions manipulating the filter. First, we performed the experiment without the filter. Then, a second experiment was performed after installing a brand-new filter. Figure 12(a) shows that the presence of the filter has an effect of filtration efficiency, lowering its value from 80 % to 60 %. The figure shows that even without a filter the recirculation mode provides a sort of filtration. This result suggests that part of the filtration is made by the filter and part is given by other devices in the HVAC system, *i.e.* a fraction of the pollutants is captured by the evaporator fins, or by the ducts between the cabin and the evaporator. Curves for fresh-air mode show filtration efficiency around zero for both the cases (no filter and with a filter), with more fluctuations for the case without a filter. Then, the presence of the filter does not improve the air quality within the cabin both by using a filter and by not using it.

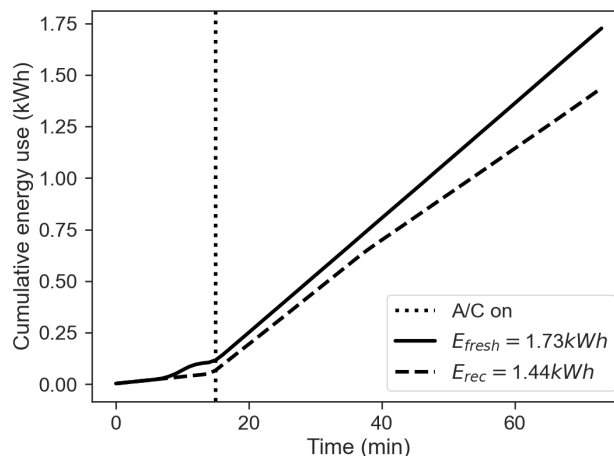
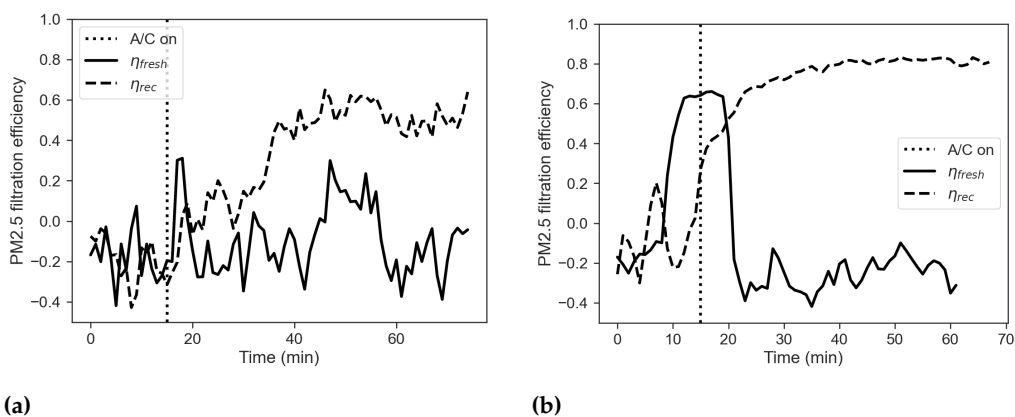


Figure 23. Cumulative energy use, comparison between fresh-air mode (solid line) and recirculation (dashed line) mode.

352 mode provides a sort of filtration. This result suggests that part of the filtration is made
 353 by the filter and part is given by other devices in the HVAC system, *i.e.* a fraction of the
 354 pollutants is captured by the evaporator fins, or by the ducts between the cabin and the
 355 evaporator. Curves for fresh-air mode show filtration efficiency around zero for both
 356 the cases (no filter and with a filter), with more fluctuations for the case without a filter.
 357 Then, the presence of the filter does not improve the air quality within the cabin both by
 358 using a filter and by not using it.



(a) **(b)**
Figure 24. Filtration efficiency, comparison between fresh-air mode (solid line) and recirculation (dashed line) mode, with 24(a) no cabin filter installed and 24(b) with brand new cabin filter installed.

359 4. Discussion

360 In this paper, a characterisation of the air quality within the cabin of a battery electric
 361 vehicle (BEV) has been shown. The temperature, PM and VOC concentrations have
 362 been measured by means of a low-cost Arduino-based system of sensors. Comparisons
 363 between the air quality obtained in the cabin during different configuration modes of
 364 the air-ventilation system have been carried out.

365 The main differences outlined are related to the fresh-air and recirculation configu-
 366 rations. The temperature distributions have been monitored and analysed along with the
 367 energy consumption of the HVAC system. The results show that, while PMs are filtered,
 368 VOCs concentrations tend to increase during operation in recirculation mode. At the
 369 same time, the HVAC energy consumption in recirculation mode after 1 h of operation is
 370 about 72 % and 82 % of the energy consumption observed in fresh-air mode for heating

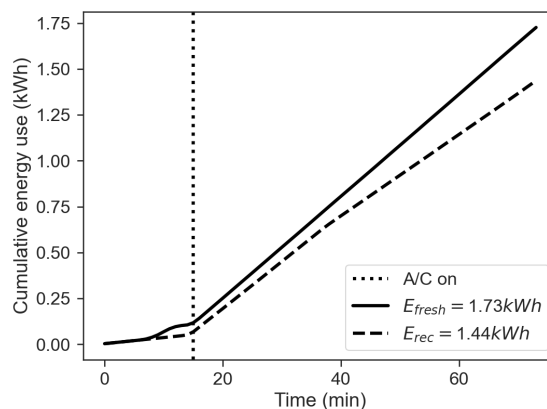


Figure 11. Cumulative energy use, comparison between fresh-air mode (solid line) and recirculation (dashed line) mode.

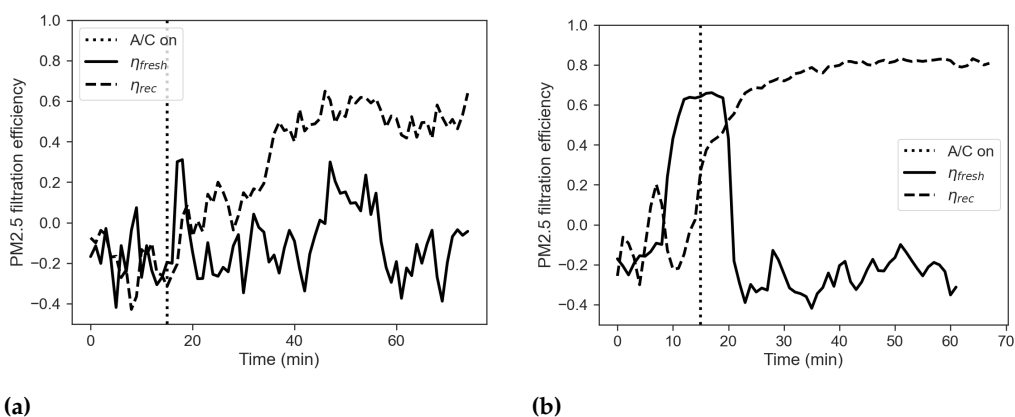


Figure 12. Filtration efficiency, comparison between fresh-air mode (solid line) and recirculation (dashed line) mode, with 12(a) no cabin filter installed and 12(b) with brand new cabin filter installed.

349 4. Conclusions

350 In this paper, a characterisation of the air quality within the cabin of a battery
 351 electric vehicle (BEV), together with real time measurements of HVAC system energy
 352 consumption has been presented. The temperature, PM_{2.5} and VOC concentrations have
 353 been measured by means of a low-cost Arduino-based system of sensors. Comparisons
 354 between the air quality obtained in the cabin during different configuration modes of
 355 the air-ventilation system have been carried out.

356 The results show that, while PMs are filtered, VOCs concentrations increase during
 357 operation in recirculation mode. At the same time, the HVAC energy consumption
 358 in recirculation mode is about 70% of the energy consumption measured in fresh-air
 359 mode during heating operation. In cooling operation, the HVAC energy consumption in
 360 recirculation mode is about 80% of the energy consumption measured in fresh-air mode.

361 Recirculation mode is found to be the best choice for BEVs, both for reducing some
 362 pollutants concentrations and for saving energy. The use of a new filter can improve the
 363 filtration efficiency in recirculation mode.

364 The methodology presented in this paper, applied to a Nissan Leaf Acenta 40 kWh,
 365 can be easily extended to other vehicles. This approach is very important for BEVs
 366 as the parameters analysed are crucial for these vehicles. In fact, the air quality is
 367 strongly related to air-circulation modes, such as the fresh-air or recirculation modes.
 368 The recirculation mode should be chosen for energy saving in order to extend the BEV
 369 drive range, but a fresh-air mode is needed in some cases, to ensure low concentrations

371 and cooling operation respectively. Moreover, cabin over temperature issues are ob-
372 served in both fresh-air and recirculation mode. This result, despite being consistent in
373 terms temperature different, has an opposite impact on system performance depending
374 on the season considered; in the winter case a temperature higher than the set-point
375 might be interpreted as a waste of energy and could be avoided, in the summer case a
376 higher than set-point temperature might suggest that the HVAC system is undersized
377 for cooling operation.

378 Temperature gradients inside the cabin pose also questions about the correct lo-
379 cation of the measurement point. On one hand, discrepancies are significant and can
380 approach 15 C; on the other hand, their uniform behaviour after the startup phase
381 could suggest that a reduction of the measuring points could be attempted without
382 compromising spatio-temporal resolution.

383 Thermal aspects are crucial for determining the energy consumed by the inbuilt
384 climate control system outside, and outside air temperature is not the only parameter
385 of interest; also solar irradiance and wind speed have an impact on cabin temperature.
386 Future studies must address also these quantities to possibly obtain a proper model of
387 the vehicle cabin.

388 Recirculation mode remains the best choice for BEVs both for reducing some pol-
389 lutants concentrations and for saving energy. The use of a new filter can improve the
390 filtration efficiency in recirculation mode, while does not make difference in fresh-air
391 mode. These results need to be compared with the CO₂ concentrations obtained in
392 recirculation mode, in order to find the minimum energy consumption together with
393 the best air quality within the cabin in a win-win approach. An optimal data-driven
394 duty-cycle of recirculation activation and deactivation could be defined to optimize both
395 comfort needs and energy consumption.

396 **Author Contributions:** Individual author contributions to the present research paper can be
397 summarized as follows: Conceptualization, L.R., B.P., G.S. and P.G.; methodology, L.R. and P.G.;
398 software, P.G., L.R. and D.A.; validation, B.P., G.S. and G.P.; formal analysis, L.R. and P.G.; investi-
399 gation, L.R.; resources, P.G., B.P., G.S. and G.P.; data curation, L.R. and P.G.; writing—original draft
400 preparation, L.R., P.G. and D.A.; writing—review and editing, B.P., G.S. and G.P.; visualization,
401 L.R.; supervision, B.P. and G.S.; project administration, B.P.; funding acquisition, B.P. All authors
402 have read and agreed to the published version of the manuscript.

403 **Funding:** This work has received funding from the LiBER project, funded by Emilia-Romagna
404 region (Italy), POR-FESR 2014-2020.

405 **Acknowledgments:** The Authors want to thank Maurizio Chendi for the precious help in the
406 set-up of the experiments.

407 **Conflicts of Interest:** The authors declare no conflict of interest. The funders had no role in the
408 design of the study; in the collection, analyses, or interpretation of data; in the writing of the
409 manuscript, or in the decision to publish the results.

410 Abbreviations

411 The following abbreviations are used in this manuscript:
412

of pollutants within the cabin. Control systems should consider these results in order to manage the HVAC system operation in a win-win approach for BEVs.

Supplementary Materials: The following are available online at <https://www.mdpi.com/1424-8220/11/1/0/s1>, Figure S1: Heating temperature profiles, fresh-air mode, Figure S2: Heating temperature difference profiles, fresh-air mode, Figure S3: Heating temperature profiles, recirculation mode, Figure S4: Heating temperature difference profiles, recirculation mode, Figure S5: Cooling temperature profiles, fresh-air mode, Figure S6: Cooling temperature difference profiles, fresh-air mode, Figure S7: Cooling temperature profiles, recirculation mode, Figure S8: Cooling temperature difference profiles, recirculation mode.

Author Contributions: Individual author contributions to the present research paper can be summarized as follows: Conceptualization, L.R., B.P., G.S. and P.G.; methodology, L.R. and P.G.; software, P.G., L.R. and D.A.; validation, B.P., G.S. and G.P.; formal analysis, L.R. and P.G.; investigation, L.R.; resources, P.G., B.P., G.S. and G.P.; data curation, L.R. and P.G.; writing—original draft preparation, L.R., P.G. and D.A.; writing—review and editing, B.P., G.S. and G.P.; visualization, L.R.; supervision, B.P. and G.S.; project administration, B.P.; funding acquisition, B.P. All authors have read and agreed to the published version of the manuscript.

Funding: This work has received funding from the LiBER project, funded by Emilia-Romagna region (Italy), POR-FESR 2018-2020.

Acknowledgments: The Authors want to thank Maurizio Chendi for the precious help in the set-up of the experiments.

Conflicts of Interest: The authors declare no conflict of interest. The funders had no role in the design of the study; in the collection, analyses, or interpretation of data; in the writing of the manuscript, or in the decision to publish the results.

Abbreviations

The following abbreviations are used in this manuscript:

BEV	Battery Electric Vehicle
HVAC	Heating, Ventilation and Air Conditioning
A/C	Air Conditioning
PTC	Positive Temperature Coefficient
IAQ	Internal Air Quality
OBD	On-Board Diagnostic
MY	Model Year
I/O	Inside/Outside
NTC	Negative Temperature Coefficient
PM	Particulate Matter
VOC	Volatile Organic Compounds

References

1. Russi, L.; Guidorzi, P.; Pulvirenti, B.; Semprini, G.; Aguiari, D.; Pau, G. Air quality and comfort characterisation within an electric vehicle cabin. 2021 IEEE International Workshop on Metrology for Automotive (MetroAutomotive), 2021, pp. 169–174. doi:10.1109/MetroAutomotive50197.2021.9502853.
2. Optemus - Optemus | Optimised and Systematic Energy Management in Electric Vehicles. <http://www.optemus.eu/>.
3. ISO. *BS ISO/DIS 14505-4:2020. Ergonomics of the thermal environment – Evaluation of thermal environments in vehicles – Part 4: Determination of the equivalent temperature by means of a numerical manikin*; BSI Standards Publication, 2020.
4. Nilsson, H. Comfort Climate Evaluation with Thermal Manikin Methods and Computer Simulation Models. PhD thesis, Bygghvetenskap, 2004.
5. Zhang, C.; Shen, K.; Yang, F.; Yuan, C. Multiphysics Modeling of Energy Intensity and Energy Efficiency of Electric Vehicle Operation. *Procedia CIRP* **2019**, *80*, 322–327. doi: 10.1016/j.procir.2019.01.058.

BEV	Battery Electric Vehicle
HVAC	Heating, Ventilation and Air Conditioning
IAQ	Internal Air Quality
OBD	On-Board Diagnostic
NTC	Negative Temperature Coefficient
PM	Particulate Matter
VOC	Volatile Organic Compounds
FTL	Front Top Left
FTC	Front Top Center
FTR	Front Top Right
FML	Front Middle Left
FMC	Front Middle Center
413 FMR	Front Middle Right
FBL	Front Bottom Left
FBC	Front Bottom Center
FBR	Front Bottom Right
BTL	Back Top Left
BTC	Back Top Center
BTR	Back Top Right
BML	Back Middle Left
BMC	Back Middle Center
BMR	Back Middle Right
BBL	Back Bottom Left
BBC	Back Bottom Center
BBR	Back Bottom Right

414 References

- 415 1. Russi, L.; Guidorzi, P.; Pulvirenti, B.; Semprini, G.; Aguiari, D.; Pau, G. Air quality and
416 comfort characterisation within an electric vehicle cabin. 2021 IEEE International Workshop
417 on Metrology for Automotive (MetroAutomotive), 2021, pp. 169–174. doi:10.1109/MetroAu-
418 tomotive50197.2021.9502853.
- 419 2. Atkinson, W.J.; Hill, W.R.; Mathur, G.D. The Impact of Increased Air Recirculation on Interior
420 Cabin Air Quality. SAE Technical Paper. SAE International, 2017. doi:10.4271/2017-01-0169.
- 421 3. Pham, L.; Molden, N.; Boyle, S.; Johnson, K.; Jung, H. Development of a Standard Testing
422 Method for Vehicle Cabin Air Quality Index. *SAE International Journal of Commercial Vehicles*
423 **2019**, *12*. doi:10.4271/02-12-02-0012.
- 424 4. M. Gerboles.; L. Spinelle.; A. Borowiak. Measuring air pollution with low-cost sensors.
425 [https://ec.europa.eu/jrc/en/publication/brochures-leaflets/measuring-air-pollution-
426 low-cost-sensors](https://ec.europa.eu/jrc/en/publication/brochures-leaflets/measuring-air-pollution-low-cost-sensors), accessed on 2021-03-05.
- 427 5. Karami, M.; McMorrow, G.V.; Wang, L. Continuous monitoring of indoor environmental
428 quality using an Arduino-based data acquisition system. *Journal of Building Engineering* **2018**,
429 *19*, 412–419. doi:10.1016/j.jobbe.2018.05.014.
- 430 6. Kumar Sai, K.B.; Mukherjee, S.; Parveen Sultana, H. Low Cost IoT Based Air Quality
431 Monitoring Setup Using Arduino and MQ Series Sensors With Dataset Analysis. *Procedia*
432 *Computer Science* **2019**, *165*, 322–327. doi:10.1016/j.procs.2020.01.043.
- 433 7. Doyle, A.; Muneer, T. Energy consumption and modelling of the climate control system in
434 the electric vehicle. *Energy Exploration & Exploitation* **2019**, *37*, 519–543. Publisher: SAGE
435 Publications Ltd STM, doi:10.1177/0144598718806458.
- 436 8. Doyle, A.; Muneer, T.; Smith, I. A review of the thermal performance of electric vehicles. 2015
437 IEEE International Transportation Electrification Conference (ITEC), 2015, pp. 1–5. ISSN:
438 null, doi:10.1109/ITEC-India.2015.7386922.
- 439 9. Koritsoglou, K.; Christou, V.; Ntritsos, G.; Tsoumanis, G.; Tsiouras, M.G.; Giannakeas,
440 N.; Tzallas, A.T. Improving the Accuracy of Low-Cost Sensor Measurements for Freezer
441 Automation. *Sensors* **2020**, *20*, 6389. Number: 21 Publisher: Multidisciplinary Digital
442 Publishing Institute, doi:10.3390/s20216389.
- 443 10. ISO. *BS ISO 16000-37:2019. Indoor Air - Part 37: Measurement of PM_{2,5} mass concentration*; BSI
444 Standards Publication, 2019.

- 412 6. Organization, W.H., Ed. *WHO guidelines for indoor air quality: household fuel combustion*; World
413 Health Organization: Geneva, Switzerland, 2014. OCLC: ocn927460179.
- 414 7. Organization, W.H., Ed. *Who guidelines for indoor air quality: selected pollutants*; WHO:
415 Copenhagen, 2010. OCLC: ocn696099951.
- 416 8. Heseltine, E.; Rosen, J.; Organization, W.H., Eds. *WHO guidelines for indoor air quality:
417 dampness and mould*; WHO: Copenhagen, 2009. OCLC: ocn429024432.
- 418 9. Settimo, G.; Manigrasso, M.; Avino, P. Indoor Air Quality: A Focus on the European
419 Legislation and State-of-the-Art Research in Italy. *Atmosphere* **2020**, *11*, 370. Number: 4
420 Publisher: Multidisciplinary Digital Publishing Institute, doi:10.3390/atmos11040370.
- 421 10. Heo, K.J.; Noh, J.W.; Lee, B.U.; Kim, Y.; Jung, J.H. Comparison of filtration performance
422 of commercially available automotive cabin air filters against various airborne pollutants.
423 *Building and Environment* **2019**, *161*, 106272. doi:10.1016/j.buildenv.2019.106272.
- 424 11. Atkinson, W.J.; Hill, W.R.; Mathur, G.D. The Impact of Increased Air Recirculation on Interior
425 Cabin Air Quality. SAE Technical Paper. SAE International, 2017. doi:10.4271/2017-01-0169.
- 426 12. Vartires, A.; Colda, I.; Topoc, S.M. Research on thermal comfort and indoor air pollution in
427 a passenger car. 2017 International Conference on ENERGY and ENVIRONMENT (CIEM),
428 2017, pp. 148–152. doi:10.1109/CIEM.2017.8120872.
- 429 13. Pham, L.; Molden, N.; Boyle, S.; Johnson, K.; Jung, H. Development of a Standard Testing
430 Method for Vehicle Cabin Air Quality Index. *SAE International Journal of Commercial Vehicles*
431 **2019**, *12*. doi:10.4271/02-12-02-0012.
- 432 14. Grady, M.L.; Jung, H.; chul Kim, Y.; Park, J.K.; Lee, B.C. Vehicle Cabin Air Quality with
433 Fractional Air Recirculation. SAE 2013 World Congress & Exhibition, 2013, pp. 2013-01-1494.
434 doi:10.4271/2013-01-1494.
- 435 15. Alger, J.A.; Buss, A.R.; Creasman, J.D.; Hoy, J.R. Automatic vehicle climate control based on
436 predicted air quality. US US10226982B2, March, 2019.
- 437 16. NEWMAN, A. Automatic vehicle cabin air filtration system. US US10245924B2, April, 2019.
- 438 17. Li, C.; Brewer, E.; Pham, L.; Jung, H. Reducing Mobile Air Conditioner (MAC) Power
439 Consumption Using Active Cabin-Air-Recirculation in A Plug-In Hybrid Electric Vehicle
440 (PHEV). *World Electric Vehicle Journal* **2018**, *9*, 51. Number: 4 Publisher: Multidisciplinary
441 Digital Publishing Institute, doi:10.3390/wevj9040051.
- 442 18. M. Gerboles.; L. Spinelle.; A. Borowiak. Measuring air pollution with low-cost sensors.
443 [https://ec.europa.eu/jrc/en/publication/brochures-leaflets/measuring-air-pollution-
444 low-cost-sensors](https://ec.europa.eu/jrc/en/publication/brochures-leaflets/measuring-air-pollution-low-cost-sensors), accessed on 2021-03-05.
- 445 19. Rüffer, D.; Hoehne, F.; Bühler, J. New Digital Metal-Oxide (MOx) Sensor Platform. *Sensors*
446 (*Basel, Switzerland*) **2018**, *18*. doi:10.3390/s18041052.
- 447 20. Yasuda, T.; Yonemura, S.; Tani, A. Comparison of the Characteristics of Small Commercial
448 NDIR CO₂ Sensor Models and Development of a Portable CO₂ Measurement Device. *Sensors*
449 **2012**, *12*, 3641–3655. Number: 3 Publisher: Molecular Diversity Preservation International,
450 doi:10.3390/s120303641.
- 451 21. Tryner, J.; Mehaffy, J.; Miller-Lionberg, D.; Volckens, J. Effects of aerosol type and simulated
452 aging on performance of low-cost PM sensors. *Journal of Aerosol Science* **2020**, *150*, 105654.
453 doi:10.1016/j.jaerosci.2020.105654.
- 454 22. Kondaveeti, H.K.; Kumaravelu, N.K.; Vanambathina, S.D.; Mathe, S.E.; Vappangi, S. A sys-
455 tematic literature review on prototyping with Arduino: Applications, challenges, advantages,
456 and limitations. *Computer Science Review* **2021**, *40*, 100364. doi:10.1016/j.cosrev.2021.100364.
- 457 23. Karami, M.; McMorrow, G.V.; Wang, L. Continuous monitoring of indoor environmental
458 quality using an Arduino-based data acquisition system. *Journal of Building Engineering* **2018**,
459 *19*, 412–419. doi:10.1016/j.jobe.2018.05.014.
- 460 24. Kumar Sai, K.B.; Mukherjee, S.; Parveen Sultana, H. Low Cost IoT Based Air Quality
461 Monitoring Setup Using Arduino and MQ Series Sensors With Dataset Analysis. *Procedia*
462 *Computer Science* **2019**, *165*, 322–327. doi:10.1016/j.procs.2020.01.043.
- 463 25. Doyle, A.; Muneer, T. Energy consumption and modelling of the climate control system in
464 the electric vehicle. *Energy Exploration & Exploitation* **2019**, *37*, 519–543. Publisher: SAGE
465 Publications Ltd STM, doi:10.1177/0144598718806458.
- 466 26. Doyle, A.; Muneer, T.; Smith, I. A review of the thermal performance of electric vehicles. 2015
467 IEEE International Transportation Electrification Conference (ITEC), 2015, pp. 1–5. ISSN:
468 null, doi:10.1109/ITEC-India.2015.7386922.
- 469 27. Koritsoglou, K.; Christou, V.; Ntritsos, G.; Tsoumanis, G.; Tsiouras, M.G.; Giannakeas,
470 N.; Tzallas, A.T. Improving the Accuracy of Low-Cost Sensor Measurements for Freezer

- 445 11. ISO. *BS ISO 12219-1:2012. Interior air of road vehicles — Part 1: Whole vehicle test chamber*
446 —*Specification and method for the determination of volatile organic compounds in cabin interiors*;
447 BSI Standards Publication, 2012.
- 448 12. Aguiari, D. *Exploring Computing Continuum in IoT Systems: Sensing, Communicating and*
449 *Processing at the Network Edge*. PhD thesis, University of Cagliari - Sorbonne Université,
450 2021. Cap. 7.
- 451 13. Christ, R.D.; Wernli, R.L. *Sensor Theory*. In *The ROV Manual*; Elsevier, 2014; pp. 297–326.
452 doi:10.1016/B978-0-08-098288-5.00012-9.
- 453 14. Guthrie, W.F. NIST/SEMATECH e-Handbook of Statistical Methods (NIST Handbook
454 151). <https://www.itl.nist.gov/div898/handbook/>,
455 accessed on 2021-03-18. doi: 10.18434/M32189.
- 456 15. Guidelines for Reliable Long Line 1-Wire Networks. [https://www.maximintegrated.com/
457 en/design/technical-documents/tutorials/1/148.html](https://www.maximintegrated.com/en/design/technical-documents/tutorials/1/148.html), accessed on 2021-10-14.
- 458 16. Sensortec, B. BME280 Combined humidity and pressure sensor. *Bosch Sensortec* **2018**.
- 459 17. Li, J.; Li, H.; Ma, Y.; Wang, Y.; Abokifa, A.A.; Lu, C.; Biswas, P. Spatiotemporal distribution
460 of indoor particulate matter concentration with a low-cost sensor network. *Building and*
461 *Environment* **2018**, *127*, 138–147. doi:10.1016/j.buildenv.2017.11.001.
- 462 18. Tryner, J.; Mehaffy, J.; Miller-Lionberg, D.; Volckens, J. Effects of aerosol type and simulated
463 aging on performance of low-cost PM sensors. *Journal of Aerosol Science* **2020**, *150*, 105654.
464 doi:10.1016/j.jaerosci.2020.105654.
- 465 19. Rüffer, D.; Hoehne, F.; Bühler, J. New Digital Metal-Oxide (MOx) Sensor Platform. *Sensors*
466 *(Basel, Switzerland)* **2018**, *18*. doi:10.3390/s18041052.
- 467 20. Nilsson, H. *Comfort Climate Evaluation with Thermal Manikin Methods and Computer*
468 *Simulation Models*. PhD thesis, Bygghvetenskap, 2004.
- 469 21. Heo, K.J.; Noh, J.W.; Lee, B.U.; Kim, Y.; Jung, J.H. Comparison of filtration performance
470 of commercially available automotive cabin air filters against various airborne pollutants.
471 *Building and Environment* **2019**, *161*, 106272. doi:10.1016/j.buildenv.2019.106272.
- 472 22. Kim, Y.c.; Park, J.K.; Lee, B.C.; Grady, M.L.; Jung, H. Vehicle Cabin Air Quality with Fractional
473 Air Recirculation. SAE 2013 World Congress & Exhibition. SAE International, 2013. doi:
474 <https://doi.org/10.4271/2013-01-1494>.
- 475 23. Li, C.; Brewer, E.; Pham, L.; Jung, H. Reducing Mobile Air Conditioner (MAC) Power
476 Consumption Using Active Cabin-Air-Recirculation in A Plug-In Hybrid Electric Vehicle
477 (PHEV). *World Electric Vehicle Journal* **2018**, *9*, 51. Number: 4 Publisher: Multidisciplinary
478 Digital Publishing Institute, doi:10.3390/wevj9040051.
- 479 24. NEWMAN, A. Automatic vehicle cabin air filtration system. US US10245924B2, April, 2019.
- 480 25. Vartires, A.; Colda, I.; Topoc, S.M. Research on thermal comfort and indoor air pollution in
481 a passenger car. 2017 International Conference on ENERGY and ENVIRONMENT (CIEM),
482 2017, pp. 148–152. doi:10.1109/CIEM.2017.8120872.
- 483 26. Alger, J.A.; Buss, A.R.; Creasman, J.D.; Hoy, J.R. Automatic vehicle climate control based on
484 predicted air quality. US US10226982B2, March, 2019.
- 485 27. Kondaveeti, H.K.; Kumaravelu, N.K.; Vanambathina, S.D.; Mathe, S.E.; Vappangi, S. A sys-
486 tematic literature review on prototyping with Arduino: Applications, challenges, advantages,
487 and limitations. *Computer Science Review* **2021**, *40*, 100364. doi:10.1016/j.cosrev.2021.100364.
- 488 28. Yasuda, T.; Yonemura, S.; Tani, A. Comparison of the Characteristics of Small Commercial
489 NDIR CO2 Sensor Models and Development of a Portable CO2 Measurement Device. *Sensors*
490 **2012**, *12*, 3641–3655. Number: 3 Publisher: Molecular Diversity Preservation International,
491 doi:10.3390/s120303641.
- 492 29. Organization, W.H., Ed. *Who guidelines for indoor air quality: selected pollutants*; WHO:
493 Copenhagen, 2010. OCLC: ocn696099951.
- 494 30. Organization, W.H., Ed. *WHO guidelines for indoor air quality: household fuel combustion*; World
495 Health Organization: Geneva, Switzerland, 2014. OCLC: ocn927460179.
- 496 31. Heseltine, E.; Rosen, J.; Organization, W.H., Eds. *WHO guidelines for indoor air quality:*
497 *dampness and mould*; WHO: Copenhagen, 2009. OCLC: ocn429024432.
- 498 32. Settimo, G.; Manigrasso, M.; Avino, P. Indoor Air Quality: A Focus on the European
499 Legislation and State-of-the-Art Research in Italy. *Atmosphere* **2020**, *11*, 370. Number: 4
500 Publisher: Multidisciplinary Digital Publishing Institute, doi:10.3390/atmos11040370.
- 501 33. Zhang, C.; Shen, K.; Yang, F.; Yuan, C. Multiphysics Modeling of Energy Intensity and
502 Energy Efficiency of Electric Vehicle Operation. *Procedia CIRP* **2019**, *80*, 322–327. doi:
503 10.1016/j.procir.2019.01.058.

- 471 Automation. *Sensors* **2020**, *20*, 6389. Number: 21 Publisher: Multidisciplinary Digital
472 Publishing Institute, doi:10.3390/s20216389.
- 473 28. ISO. *BS ISO 16000-37:2019. Indoor Air - Part 37: Measurement of PM_{2,5} mass concentration*; BSI
474 Standards Publication, 2019.
- 475 29. ISO. *BS ISO 12219-1:2012. Interior air of road vehicles — Part 1: Whole vehicle test chamber*
476 *—Specification and method for the determination of volatile organic compounds in cabin interiors*;
477 BSI Standards Publication, 2012.
- 478 30. Aguiari, D. Exploring Computing Continuum in IoT Systems: Sensing, Communicating and
479 Processing at the Network Edge. PhD thesis, University of Cagliari - Sorbonne Université,
480 2021. Cap. 7.
- 481 31. Christ, R.D.; Wernli, R.L. Sensor Theory. In *The ROV Manual*; Elsevier, 2014; pp. 297–326.
482 doi:10.1016/B978-0-08-098288-5.00012-9.
- 483 32. Guthrie, W.F. NIST/SEMATECH e-Handbook of Statistical Methods (NIST Handbook
484 151). <https://www.itl.nist.gov/div898/handbook/>,
485 accessed on 2021-03-18. doi:
10.18434/M32189.
- 486 33. Guidelines for Reliable Long Line 1-Wire Networks. [https://www.maximintegrated.com/
487 en/design/technical-documents/tutorials/1/148.html](https://www.maximintegrated.com/en/design/technical-documents/tutorials/1/148.html), accessed on 2021-10-14.
- 488 34. Sensortec, B. BME280 Combined humidity and pressure sensor. *Bosch Sensortec* **2018**.
- 489 35. Li, J.; Li, H.; Ma, Y.; Wang, Y.; Abokifa, A.A.; Lu, C.; Biswas, P. Spatiotemporal distribution
490 of indoor particulate matter concentration with a low-cost sensor network. *Building and
491 Environment* **2018**, *127*, 138–147. doi:10.1016/j.buildenv.2017.11.001.